Differences in resting state functional networks in HIV infected and uninfected children at age 7 years

by

JADRANA TOICH

TCHJAD001

In partial fulfillment of the requirements for the degree of Master of Science in Biomedical engineering.

Faculty of Health Science

UNIVERSITY OF CAPE TOWN

October, 2015

Supervisor: Prof. Ernesta Meintjes

Co-supervisors: Dr. Paul Taylor, Dr. Martha Holmes

DECLARATION

I, JADRANA TOICH, hereby declare that the work on which this thesis is based is my own original work (except where acknowledgements indicate otherwise) and that neither the whole, nor any part of it, has been, or is to be submitted for any other degree in this or any other University.

I empower the University to reproduce for the purpose of research either the whole or part of the contents of this thesis in any manner.

Signed by candidate

Signature Removed

Signature

15 / 10 / 2015

Date

ACKNOWLEDGEMENT

I hereby wish to express my sincere gratitude to the following individuals who enabled this document to be successfully completed:

- Professor Ernesta Meintjes for guidance, advice and support throughout this project
- My co-supervisors, Dr. Martha Holmes and Dr. Paul Taylor for all your assistance, ideas, knowledge, time and motivation
- Friends & family for their support

The following organizations that provided the funding for this work:

- The NRF
- Hillary and Dorothy trust fund
- NIH/NICHD

ABSTRACT

Although early administration of highly active antiretroviral therapy (HAART) in infants provides the brain some protection against HIV damage, few studies have examined the long-term effects of HIV infection and HAART on neurodevelopment, and none have measured their impact on functional brain networks in young children. We use resting state functional magnetic resonance imaging (RS-fMRI) to explore differences in functional connectivity (FC) in HIV infected children stable on HAART and in HIV uninfected children. The 9 resting state networks (RSNs) identified using independent component analysis (ICA) included the visual lingual gyrus, visual occipital gyrus, salience, dorsal attention, auditory, motor, executive control, posterior default mode network (pDMN) and default mode network (DMN). No significant group level differences were found in any RSNs using ICA. However, seed-based correlation analysis (SCA) revealed two regions where uninfected children had a higher FC compared to infected children ($p < 0.05$ corrected for multiple comparison); specifically, between a seed in the left cingulate gyrus of the DMN and the left middle frontal gyrus, and between a seed in the right middle frontal gyrus of the executive control network and the right supramarginal gyrus.

Consistent with our findings, previous RS-fMRI studies in HIV infected adults have reported reduced connectivity compared to uninfected adults in numerous DMN regions and executive control network. However, in contrast to the adult literature, in which a number of areas within the networks have been implicated, we only observed a focal effect in each of the two RSNs. Given that some of the RSNs are still undergoing major developments at age 7 years (i.e. time of scan for the children), the reduced FC may represent delayed network maturation within the infected cohort, with potential effects on cognitive functioning, information processing and memory recall abilities. Furthermore, positive associations were found between the clinical CD4/CD8 at time of enrollment and two regions within the dorsal attention and auditory networks. These results were independent of treatment arm and suggest that reduced FC in these networks at age 7 years are a result of poor immune function in early infancy (6-8 weeks of age), supporting the notion of initiating ART immediately in HIV infected infants.

TABLE OF CONTENTS

LIST OF FIGURES

LIST OF TABLES

LIST OF ABBREVIATIONS

3D	3-dimensional
AFNI	analysis of functional neuroimages
AGA	appropriate for gestational age
AIDS	acquired immune deficiency syndrome
ANOVA	analysis of variance
ART	antiretroviral treatment
ART-Def	ART deferred until CD4% < 25% in first year or CD4% < 20% thereafter, or if clinical disease progression criteria presented
ART-40W	ART initiated immediately and interrupted after 40 weeks
ART-96W	ART initiated immediately and interrupted after 96 weeks
AZT	Azidothymidine (administered as ART)
BOLD	blood oxygenated level dependent
CD	cluster of differentiation
CHER	children with HIV early antiretroviral therapy
CIPRA-SA	comprehensive international program for research on AIDS in South Africa
CNS	central nervous system
CSF	cerebrospinal fluid
CUBIC	Cape Universities Brain Imaging Center
dHb	deoxyhemoglobin
DMN	default mode network
DNA	deoxyribonucleic acid
DOF	degrees of freedom
DTI	diffusion tensor imaging
EPI	echo planar imaging
FATCAT	functional and tractographic connectivity analysis toolbox
FC	functional connectivity

FCP	functional connectome project
fMRI	functional magnetic resonance imaging
FOV	field of view
FSL	FMRIB Software Library
FWHM	full width at half maximum
GLM	general linear model
GM	grey matter
HAART	highly active anti-retroviral treatment
Hb	oxyhemoglobin
HIV	human immunodeficiency virus
IC	independent component
ICA	independent component analysis
KID-CRU	Children's Infectious Diseases Clinical Research Unit
LFF	low frequency fluctuations
LPV/r	Lopinavir/Ritonavir (administered as ART)
MELODIC	multivariate exploratory linear optimized decomposition into independent components (FSL program for ICA)
MEMPRAGE	multiecho magnetization prepared rapid gradient echo
MR	magnetic resonance
MRI	magnetic resonance imaging
MRS	magnetic resonance spectroscopy
MTCT	mother to child transmission
NP	neuropsychological measure
NVP	Nevirapine (administered as ART)
PCC	posterior cingulate cortex
PCR	polymerase-chain-reaction
PMTCT	prevention of mother to child transmission
PVL	plasma viral load

RF	radiofrequency
RNA	ribonucleic acid
RS	resting state
RSFC	resting state functional connectivity
RS-fMRI	resting state functional magnetic resonance imaging
RSN	resting state network
SA	South Africa
SCA	seed-based correlation analysis
SGA	small for gestational age
SIP	speed of information processing
SNR	signal to noise ratio
SSA	sub-Saharan Africa
TB	task-based
TE	echo time
TI	inversion time
TR	repetition time
VIF	variance inflation factor
VL	viral load
VWFD	voxel-wise framewise displacement
WM	white matter
ZDV	Zidovudine (administered as ART)

1. INTRODUCTION

Human immunodeficiency virus (HIV) and the associated acquired immune deficiency syndrome (AIDS) has been predominantly transformed from a fatal to a chronic disease by the development and availability of highly active antiretroviral therapy (HAART). HAART has been responsible for significantly improving the mortality and morbidity rates of HIV infected patients around the globe (Eisenhut, 2012; Lindsey et al., 2007; Koekkoek et al., 2006; Saitoh et al., 2006). However, unlike the virus itself, the therapy is not able to effectively penetrate the blood-brain barrier of the central nervous system (CNS). Therefore, the virus is able to use the brain as a sanctuary site for a persistent reservoir, resulting in long-term damage and delayed neurodevelopment (Laughton et al., 2013; Smith et al., 2012; Patel, 2009; Letendre et al., 2008; Van Rie et al., 2006; Shanbhag et al., 2005).

Over 3 million children worldwide are currently living with HIV, and the majority of these children reside in sub-Saharan Africa (SSA) (WHO, 2013a). The neurological effects of HIV tend to be most severe in the developing brains of infants and children because of the immaturity of their nervous and immune systems (Van Rie et al., 2009; Chakraborty, 2008; Van Rie et al., 2006; Wachsler-Felder & Golden, 2002).

Starting in 2005, the Comprehensive International Program for Research on AIDS in South Africa (CIPRA-SA) initiated the 'Children with HIV early antiretroviral therapy' (CHER) trial, which investigated HAART strategies in infants and children from resource limited settings over a 5-year period (Cotton et al., 2013; Violari et al., 2008). The results showed that infant mortality was reduced by 76% and HIV progression by 75% in infants receiving HAART from an early age (mean age of 7 weeks). As a result, the South African Antiretroviral Treatment Guidelines (2013) now also recommend ART initiation to all children below the age of 5 years.

For pediatric HIV patients, the manifestations of HIV are particularly dependent on the age of the child, as their brains are developing at a rapid rate during early childhood (Van Rie et al., 2006; Wachsler-Felder & Golden, 2002). Previous pediatric HIV clinical studies have generally had a large age difference within their examined cohorts (5-10 years), which makes it difficult to compare neurodevelopmental and neurocognitive assessment across participants (Palchetti et al., 2012; Thomaidis et al., 2010; Koekkoek et al., 2008; Saitoh et al., 2006; Miziara et al., 2006; Koekkoek et al., 2006; Chirboga et al., 2005; Shanbhag et al., 2005; Tangsinmankong et al., 2004; Fishkin et al., 2000; Raskino et al., 1999; Kline et al., 1998; Tardieu et al., 1995; Diamond

et al., 1987). Furthermore, the majority of pediatric HIV studies conducted to date have been set in developed countries, where contextual factors differ greatly in comparison to those of developing countries, in which the majority of infections occur.

Very little is known about the neurological effects of HIV within children who are stable on HAART (Hoare et al., 2014; Laughton et al., 2013; Diniz et al., 2011) as many pediatric HIV studies have used HAART-naïve children and the studies that have included children on HAART have a very heterogeneous nature regarding the HAART initiation times, length of HAART usage, and the regimens being used (see, e.g. Sherr et al., 2009).

In the present study we aim to contribute to the understanding of early brain development in HIV infected children who are stable on HAART using non-invasive magnetic resonance imaging (MRI) of a well-characterized pediatric cohort. MRI has proved to be valuable in studying several disorders, as it provides evidence of associated brain deficits which can be related to clinical and behavioral outcomes. Furthermore, functional MRI (fMRI) can be used as a biomarker for neurocognitive changes and associated behavioral outcomes. In this study, we are using resting state fMRI (RS-fMRI) specifically, whereby several functional brain networks can be simultaneously studied from one short acquisition (approximately 6 minutes). In addition, RS-fMRI does not require task-based (TB) or performance-based metrics, making it ideal for pediatric studies as this eliminates concerns of potentially confounding factors, such as attention, task performance, and language comprehension that may be more problematic in a pediatric cohort.

For this study, RS-fMRI data acquired in 7 year old children are used to examine differences in functional brain connectivity between HIV infected children, who are stable on HAART (i.e. viral load (VL) suppressed), and HIV uninfected children from the same community and ethnic group. In addition to localizing regions of differing functional connectivity (FC), we also relate RS-fMRI values with the clinical measure, CD4/CD8 (the ratio of CD4 and CD8 counts), taken at the time of enrollment. This study will improve our understanding of the potential effects of HIV infection, as well as how FC differences relate to clinical measures.

A major strength of this study is the fact that the cohort of children is well-characterized, since their mothers were recruited by the CHER study during pregnancy, and the children have been closely monitored since birth. Specifically, the children have detailed clinical records from birth, they have received standard HAART regimens, and the participants were recruited from similar socio-demographic and economic backgrounds. The HIV uninfected controls were also

recruited from the same community for an interlinking vaccine trial. For all participants, the neuroimaging data were acquired within 6 months of their 7th birthday, to ensure a narrow age range.

To date, no studies have used RS-fMRI to study the intrinsic functional brain connectivity of HIV infected children. The most common findings from other pediatric HIV neuroimaging studies include: ventricular enlargement, cortical and subcortical atrophy, calcification of the basal ganglia and corpus callosum, as well as lesions and volume reductions in the frontal white matter (WM) (Hoare et al., 2014; Sarma et al., 2013; Hoare et al., 2012; Prado et al., 2011; Tahan et al., 2006; Martin et al., 2006; Nozyce et al., 2006; Bruck et al., 2001; Wolters et al., 1995; Pavlakis et al., 1995). However, these studies differ from this study as the age range of participants were usually quite wide, treatments were often not controlled for, and the viral loads were not always suppressed in the infected participants. Findings from pediatric HIV clinical studies primarily include cognitive delay and motor deficits, along with impaired language function, failure to reach developmental milestones, and behavioral problems in HIV infected children (Laughton et al., 2013; Eisenhut, 2012; Koekkoek et al., 2008; Lindsey et al., 2007; Van Rie et al., 2006; Nozyce et al., 2006; Smith et al., 2006; Wachsler-Felder & Golden, 2002; Bruck et al., 2001; Chase et al., 2000; Fishkin et al., 2000; Raskino et al., 1999; Tardieu et al., 1995; Diamond et al., 1987). Moreover, a decrease in cerebral volume has been associated with CD4 lymphocyte depletion, which represents the progression of HIV (Melrose et al., 2008; Thompson et al., 2005; Stout et al., 1998). In addition, a previous magnetic resonance spectroscopy (MRS) study, using the same children from this study, found that lower CD4 count and CD4/CD8 at enrollment were associated with both lower NAA and choline at age 5 (Mbugua et al., 2014). Based on these findings, we hypothesize that:

1. There will be decreased FC in HIV infected children compared to uninfected controls in the executive control and motor networks (these networks are explained in more detail in Section 2.2).
2. Decreases in FC at age 7 years will be associated with poorer immune health at enrolment, as indicated by a reduced clinical measure, CD4/CD8.

2. BACKGROUND THEORY

2.1 HIV EPIDEMIC

The HIV/AIDS epidemic accounted for approximately 1.5 million deaths and 2.1 million new infections recorded worldwide in 2013 (UNAIDS, 2013). The most heavily impacted region has been SSA, which contains 10% of the world's population but which also has 69% of all HIV infected adults, 92% of the world's pregnant women living with HIV and more than 90% of the total number of HIV infected children (UNAIDS, 2012). Over the last decade in SSA, there has been a decline in AIDS-related deaths by approximately 32% and in new infections by 25%. The number of newly infected children in the region has also declined by 24% between 2009 and 2011, showing the potential for eliminating new infections in children (UNAIDS, 2012). These significant reductions are largely attributed to the success of "prevention of mother-to-child transmission" (PMTCT) programs (WHO, 2013b; Kowala-Piaskowska et al., 2010).

South Africa (SA) has the highest concentration of people living with HIV worldwide, with over 10% of the population being HIV positive (Statistics South Africa, 2013). The percentage of AIDS-related deaths in SA has declined by about 7% over the last decade, and there has been a decrease in prevalence of HIV within youth (age 15 – 24) by 5.1% (Statistics South Africa, 2013). However, while the incidence of newly infected adults in SA has also decreased over the last decade, the prevalence of people living with HIV has increased in the adult population (age 15–49 years) by 0.8% (Statistics South Africa, 2013) – in part this could be due to improvements of diagnosis and treatment, enabling HIV infected persons to live longer.

The clinical features of HIV differ greatly depending on the age of the patient, the stage of progression of the virus, the transmission type and the treatment being undertaken. In general, the primary effects of HIV are due to infected astrocytes, macrophages, cluster difference 8 (CD8) and CD4 lymphocyte cells. CD4 cells play a major role in immune function by sending signals that activate the body's immune response when a virus is detected, while CD8 cells fight the virus itself. HIV invades the CD4 cells and uses them as a mechanism to multiply and spread throughout the body, resulting in immunodeficiency - allowing the virus to enter the CNS, to release neurotoxic factors and to cause neurological damage (Buttner et al., 2005; Wachsler-Felder & Golden, 2002; Bruck et al., 2001; Chase et al., 2000; Westmoreland et al., 1998).

Consequently, a decrease in immune function and CD4 lymphocyte cells along with an increase in cerebrospinal fluid (CSF) viral load and plasma viral load (PVL) are all associated with HIV

disease progression and neurological dysfunction which varies between patients (Wachsler-Felder & Golden, 2002; Broãœwers et al., 1996). Children and infants tend to be more severely impacted than adults due to the immaturity of their immune and nervous systems, which furthermore makes astrocytes more susceptible to infection (Chakraborty, 2008; Nozyce et al., 2006; Wachsler-Felder & Golden, et al., 2002).

The absolute CD4 cell numbers per blood volume (CD4 count) is most often used for diagnosis and for guiding decisions regarding treatment in HIV infected patients (Branson et al., 2014; Eisenhut, 2012; Bofill et al., 1992). When used in combination with the percentage of CD4 cells (CD4%) and the CD4/CD8, it provides an accurate means to track disease progression and/or the effectiveness of the treatment (Taylor et al., 1989; Bofill et al., 1992; Fahey et al., 1990).

There are a number of different ways that HIV can be transmitted from one infected person to another, including: direct blood contact (i.e. injections and blood transfusions), semen and vaginal secretions, and breast milk (Chakraborty, 2008). Sexual intercourse is the primary means for transmission in adults in SSA, while the high incidence of HIV infected children (under the age of 15) occurs almost entirely from mother to child transmission (MTCT), also called vertical infection (Eisenhut, 2012; Chakraborty, 2008; Wachsler-Felder & Golden, 2002).

There are 3 major stages at which MTCT typically occurs: in utero, during delivery and with breast feeding (Linguissi et al., 2012; Wachsler-Felder & Golden, 2002). In utero, the fetus is generally protected from maternal infections by a healthy placenta (Lyall, 2002); however, the HIV virus is able to cross the placenta under certain circumstances (e.g. drug use or inflammation) (Purohit et al., 2011). In 2013, the mortality rate of infants in SA was estimated to be 41.7 per 1000 live births, primarily as a result of HIV MTCT (Statistics South Africa, 2013). PMTCT practices include a caesarian section for delivery (as opposed to natural birth), alternatives to breast feeding, and HAART (Chouquet et al., 1999; Miotti et al., 1999). In resource-limited settings, providing HAART to HIV infected pregnant women has become a viable strategy whereby mothers can still give natural birth and breastfeed their children, while also reducing the risk of MTCT to less than 2% (Purohit et al., 2011). According to the UNAIDS regional fact sheet (UNAIDS, 2012), the coverage of services to prevent MTCT of HIV has reached 59% of the whole of SSA. SA, in particular, has a PMTCT coverage of more than 75% (UNAIDS, 2012).

The success of HAART has made it the standard of care for HIV infected patients (Badri et al., 2006). HAART attacks the virus at different stages of its replication cycle and has proven to

suppress viral replication while restoring immune function (CD4 count) (Diniz et al., 2011; Thomaidis et al., 2010; Saitoh et al., 2006), and its wide usage has drastically improved the morbidity and mortality rates of HIV patients (Purohit et al., 2011; Lindsey et al., 2007).

In the absence of antiretroviral-therapy (ART), children display symptoms of neurodevelopmental delays within their first year of life (particularly delays in motor and cognitive development), and disease progression significantly increases between ages 2-5 years (Smith et al., 2006; Bruck et al., 2001; Chase et al., 2000; Coplan et al., 1998; Gay et al., 1995). Children who are vertically infected with HIV display faster progression rates and earlier development of symptoms than those infected by blood products or transfusion (Chakraborty, 2008; Wachsler-Felder & Golden, 2002). The thymus is largely responsible for producing T-cells (e.g. CD4 cells) and is affected by HIV infection (Ye et al., 2004). It is most active before puberty, allowing a larger pool of cells to be infected in pediatric HIV patients (Chakraborty, 2008); this has been hypothesized as an explanation as to why accelerated neurodevelopmental delays are often observed in infants and young children with HIV (Chakraborty, 2008). However, with the implementation of HAART, the active thymus works in the child's favor with an increased ability to produce uninfected CD4 cells, which in turn causes a faster reconstitution of the immune system than in adults (Saitoh et al., 2006).

In the first cases of HAART administration, infants and children were only given HAART when HIV symptomatic infections were displayed. However, it has since been shown by a number of studies that the early initiation of HAART for infants and children is highly beneficial as it significantly reduces HIV progression and improves CD4 lymphocyte counts (Cotton et al., 2013; Diniz et al., 2011; Violari et al., 2008; Kids ART Link Collaboration, 2008; Badri et al., 2006). Subsequently, the treatment guidelines in SA have been adjusted for infants to start receiving HAART between 4-6 weeks of age, and all HIV positive children under the age of 5 are eligible for treatment, regardless of their CD4 count or disease stage (SA ART Guidelines, 2013). Additionally, and in part due to the successful application of HAART for the PMTCT, there are currently a large number of children born HIV negative who have been exposed to both HIV and HAART in utero.

Even though HAART has been shown to be very effective in suppressing HIV and related infections, the rollouts of HAART only began in 1995, and so the long-term effects of the treatment are not well known. There are still aspects of its use that need further investigation, especially concerning long-term usage (Diniz et al., 2011), such as the potential toxicity of

prenatal exposure to the developing brain, the potential long-term toxicity of antiretroviral therapy, adherence issues, and the risk of resistance to antiretroviral therapy (Wachsler-Felder & Golden, 2002). Many external factors influence the overall life trajectories of HIV infected patients, including prenatal drug exposure, poverty, prematurity, nutrition, socioeconomic status, and the home environment (Lindsey et al., 2007; Nozyce et al., 2006; Smith et al., 2006; Coscia et al., 2001; Broãœwers et al., 1996), making it difficult to definitively evaluate all of the primary and side effects of HAART from clinical studies. Longitudinal neuroimaging studies of young pediatric HIV participants born from HIV infected mothers may provide a useful means to track the important long-term developmental consequences of using HAART.

2.2 MRI TECHNIQUES

MRI is a non-invasive technique that can be used to study all regions of the body. In neuroimaging applications (our focus here), the method is capable of differentiating between, and investigating the properties of, brain tissues, such as grey matter (GM), white matter (WM) and CSF. MRI is useful for studying a large number of neurological pathologies because various sequence designs are capable of providing information about the structure, function and metabolism of localized regions of the brain. The main modalities performed with MRI are diffusion tensor imaging (DTI), MRS, structural MRI, and fMRI.

The key physical components of an MRI machine are the radiofrequency (RF) coils, gradient coils and a large magnet. For human and medical MRI applications, a magnetic field strength of 1.5T or 3T is usually used and applied in the direction of the z-plane (as determined by the scanner coordinates), which typically corresponds to inferior-superior orientation of the subject being scanned. The *z*-axis is known as the longitudinal direction, while the orthogonal *xy*-plane is known as the transverse plane. MRI works by measuring the electromagnetic energy absorbed and exuded by atoms in the body. It requires atoms that contain an odd number of protons and neutrons in the nucleus, as these have a net angular momentum and are therefore capable of behaving like small magnets. A large portion of the body (approximately 65%) and brain (approximately 85%) are made up of water molecules (Soberman et al., 1948), whereby each molecule contains two hydrogen atoms; additionally, organic molecules also contain a large amount of hydrogen atoms. As such, the hydrogen nucleus, having one proton, is frequently used in MRI and is also used in this study.

When placed in a large static magnetic field ($\mathbf{B_0}$), the magnetic dipole moment of a hydrogen nucleus precesses (i.e., the orientation of the dipole rotates, sweeping out a cone, without

translation) at a natural frequency (ω) that is proportional to the magnetic field strength and is known as the Larmor precession frequency. The Larmor precession frequency is given by Equation 1.

$$\omega = \gamma B_0 \quad (1)$$

The constant of proportionality γ is the gyromagnetic ratio (for hydrogen, 42.6 MHz/T). The bulk alignment and rotation of hydrogen nuclei creates a net magnetization (**M**) vector. When left undisturbed, the magnetization vector will be in line with, and of proportional magnitude to $\mathbf{B_0}$, and is denoted as M_0.

To generate a signal, an RF pulse is momentarily applied at the appropriate resonance frequency (i.e. at the Larmor frequency), creating an oscillating magnetic field ($\mathbf{B_1}$) at right angles to the static magnetic field ($\mathbf{B_0}$). This causes the net magnetization vector (**M**) to start precessing around $\mathbf{B_1}$, causing **M** to flip away from the longitudinal plane into the transverse plane in a spiraling motion. The flip angle (α) denotes the degree to which the magnetization is flipped away from $\mathbf{B_0}$ and is determined by the duration for which the RF pulse is applied and the amplitude of $\mathbf{B_1}$. A 90 degree flip angle rotates the magnetization fully into the transverse plane. A pulse sequence is the software that controls the timing of the RF pulses and gradients, which serve to spatially encode the signal.

Once the RF pulse has been terminated, the magnetization vector realigns with the axis of the main magnetic field ($\mathbf{B_0}$) via two independent relaxation processes, which are each characterized by a time constant that describes how the signal changes with time. Longitudinal relaxation is the process whereby M_Z grows back to its original strength M_0 by releasing the previously absorbed energy to the lattice. The time constant (T1) is defined as the time it takes for M_Z to regrow to around 63% of its maximum value after a 90 degree flip (Equation 2).

$$M_Z(t) = M_0(1-e^{-t/T1}) \quad (2)$$

Concurrently occurring is the process of transverse relaxation whereby M_{xy} decays to zero due to spin-spin interactions that cause individual spins to lose their phase coherence. The time constant (T2) is defined as the time it takes for M_{xy} to decay by roughly 63% after a 90 degree flip (Equation 3).

$$M_{xy}(t) = M_0e^{-t/T2} \quad (3)$$

The T1 and T2 values depend on the magnetic field strength and the type of tissue being imaged. In general, T1 recovers approximately 5-10 times slower than the decay of T2. The magnetic resonance (MR) image is formed by reading the amplitude and phase of the current induced in a receiving coil by the precessing transverse magnetization vector until it has fully decayed. The application of gradients is used to determine the spatial location of the signal being received via a three step process.

Slice selection is the first step, a technique used to isolate a single tissue slice to be excited by the transmitted RF pulse. Superimposing the gradient field ($\mathbf{G_f}$) on the main magnetic field ($\mathbf{B_0}$) in a certain axis results in a net magnetic field with a value of $\mathbf{B_0 - G_f}$ at one extreme, $\mathbf{B_0}$ in the center, and $\mathbf{B_0 + G_f}$ at the other extreme; and the Larmor frequency of the protons will also differ along the axis. Therefore, to excite a certain slice along the axis, an RF pulse is applied at a frequency equal to the Larmor frequency of the protons at that slice location. Altering the strength of the gradient will change the thickness of the excited slice.

The next two steps, frequency and phase encoding, are based on a similar approach to slice selection and use gradients to further localize regions within the excited slice. Frequency encoding is used to localize the column within the excited slice, by applying a gradient field in a direction perpendicular to the slice selection gradient, causing the Larmor frequency of the protons to differ across the excited slice; for phase encoding, a gradient is applied perpendicular to both the slice selection and frequency encoding gradients. The frequency encoding gradient is applied at the same time that the signal is being measured and the phase encoding gradient is applied after slice selection but before frequency encoding, causing spins in different locations to acquire a unique phase shift. Hence, the RF coils and magnet stimulate a signal from the protons throughout the brain which is read using a receiving coil and placed in a spatial frequency domain called k-space using gradient coils; translating the data from k-space into the spatial domain results in an image (Prince, 2006).

For this study, we used structural MRI and fMRI data. T1-weighted contrast, with a short repetition time (TR) and echo time (TE), was used to produce the high quality, 3 dimensional (3D) structural MRI image; these images provide excellent contrast between tissue types (GM, WM and CSF), allowing for the quantification of structural properties such as the shape, size, and integrity of GM and WM structures in the brain. Here, T2-weighted contrasts with long TR=2s and TE are used to produce the fMRI images (3D volumes collected over time) from

which brain activity is studied using the blood oxygenated level dependent (BOLD) signal as a proxy for neural activity.

The BOLD effect in fMRI is based on the concept that increased neural activity requires an increase of blood flow to the area of activation, resulting in a relative increase in oxygenated hemoglobin. Oxyhemoglobin (Hb) is diamagnetic because the iron molecule is surrounded by oxygen atoms that shield it, while deoxyhemoglobin (dHb) is paramagnetic and causes signal loss. The changes in local magnetic properties associated with the changes in Hb/dHb ratio serve as an indirect marker of underlying neural activity. An increase in BOLD signal is associated with a relative increase in Hb, and a decrease in signal is associated with relative increase in dHb; these changes in local magnetic susceptibility produce the BOLD signal contrasts (Jezzard et al., 2001).

There are a number of confounding (i.e., non-neuronal) factors within the BOLD signal that have been shown to affect connectivity measures (Rogers et al., 2007). Prominent ones include: physiological "noise" due to fluctuations in cerebral metabolism and blood flow, as well as cardiac and respiratory pulsations; gross head motions; and scanner drift (Birn et al., 2006; Smith et al., 1999; McKeown et al., 1998). It is therefore important to pre-process the fMRI data before conducting an analysis, to ensure that these confounding signals are minimized.

Analysis of fMRI data produces activation maps from the BOLD signal that portray the average level of engagement of different brain regions in a task (Rogers et al., 2007) and are used to study the functional architecture of the brain. FC is defined as the temporal correlation between the BOLD signal fluctuations in multiple spatially-independent brain regions. The organization and integrated performance of these different brain regions form a functional neural network (Rogers et al., 2007).

Functional networks are commonly studied in fMRI using either task-based (TB) or resting state (RS) experimental designs. For TB studies, the participant is required to perform a specific task during the fMRI scan, typically following some kind of ON/OFF paradigm; and the subsequent analysis investigates the correlation of BOLD signals in each voxel with the designated paradigm and each other, in an attempt to detect and delineate regions of the brain involved with the performance of the task at hand (Rogers et al., 2007). In contrast, RS studies require the participant to be "at rest" (i.e. the participant is awake and alert, but not actively engaging in an attention-demanding or goal-oriented task) and aims to extract simultaneous information about a number of large-scale neural networks that are functionally connected in the absence of

an external stimulus. For RS analysis, the low frequency fluctuation (LFF) content of the BOLD signal is of particular interest, typically in the range of 0.01-0.1Hz (Lee et al., 2012; Biswal et al., 1995) and the networks extracted are referred to as resting state networks (RSNs).

Nearly all of the large scale brain networks extracted with RS analysis have also been identified in TB functional studies, reflecting similar regionality and patterns, therefore verifying their interpretation as functional networks. The correlation values found with RS analysis tend to be slightly smaller than ones found with task based analysis (likely due to the decreased signal-to-noise ratio (SNR) of the former studies), but FC patterns in the networks remain very similar. A major advantage of using RS over TB analysis is that it does not require TB performance metrics, making it ideal for pediatric studies, as this eliminates the significant concern of attention and task performance in a pediatric cohort. In addition, no explicitly task-induced motion will be introduced, and several functional networks can be simultaneously extracted from one scanning session (Superkar et al., 2009).

Between 15 and 20 RSNs have been previously documented by researchers using resting state functional connectivity (RSFC); importantly, these networks have been reproduced consistently and reliably across subjects in a host of studies (Biswal et al., 2010; Smith et al., 2009; De Luca et al., 2006; Beckmann et al., 2005). In particular, the Functional Connectome Project (FCP) used over 1000 subjects to create templates for each of these networks and has often been used as a standard reference for comparison (Biswal et al., 2010). Furthermore, relevant for this thesis, a number of studies have robustly reproduced these RSNs in children (de Bie et al., 2012; Thomason et al., 2011; Superkar et al., 2010; Fair et al., 2008; Fair et al., 2007).

The RSNs can be grouped in different ways; broadly, they can be considered to be divided into two categories, namely: (1) higher order cognitive functions, which include the default mode network (DMN), attention, salience and executive control networks; and (1) lower-order sensorimotor functions, which include the visual, auditory and motor networks (Belcher et al., 2013; Mowinckel et al., 2012; de Bie et al., 2012; Heine et al., 2012). Researchers also divide these networks in terms of two major brain systems, namely a task-positive and a task-negative one, with the DMN being the only task-negative network (Kim et al., 2011; Kelly et al., 2008; Fox et al., 2006; Fox et al., 2005). Task-positive networks support externally-oriented processing and have consistently shown increased activation during different cognitive or attention demanding tasks; this has been observed to be coupled with a deactivation from the task-negative network, which is responsible for internally-oriented processing. Therefore, these two

groups of networks are anti-correlated and hypothesized to work in modular fashion to maintain a balance between responding to the external stimulus and internal processing (Kim et al., 2011; Biswal et al., 2010).

Even though there are no exact boundaries for a given RSN (and some networks can be observed to be split and divided in different ways in various studies), there are typically observed sets of regions associated with a given network. Figure 1 a,b illustrates this where the DMN is split into its orbitofrontal and posterior components, respectively, and both components together form the complete DMN. Regions of the brain that compromise the DMN have consistently been found to be most active during the RS (Long et al., 2008; Fransson, 2005; Greicius et al., 2003; Raichle et al., 2001) and include the precuneus, anterior cingulate gyrus, posterior cingulate cortex (PCC), medial prefrontal cortex, orbitofrontal gyrus, parahippocampal gyrus, inferolateral temporal cortex, and lateral parietal cortex (Andrews-Hanna et al., 2010; Greicius et al., 2003; Raichle et al., 2001).

Research has shown that the DMN acts as a central hub of transient functional interactions between multiple RSNs, i.e., it has been implicated in aiding intranetwork communication (Pasquale et al., 2012). As a whole, it has been suggested that the network is responsible for functions such as introspective thought (Andrews-Hanna et al., 2010; Fransson, 2006), self-reflection (Johnson et al., 2002), retrieval and manipulation of episodic memories and semantic knowledge, integrating cognitive and emotional processing (Greicius et al., 2003) and monitoring and responding to the external and internal environment (Raichle et al., 2001). It has also been found to be active during passive sensory processing states (e.g. auditory or visual processing), which require a low cognitive demand (Greicius et al., 2004).

In contrast to the DMN, the executive control network (see Figure 1c) is most active when the participant in involved in a goal-oriented or attention-demanding task. It is responsible for various cognitive functions, including the initiation, maintenance and regulation of attention (Dosenbach et al., 2008), along with concentration, processing speed, response inhibition, working memory, response planning and cognitive flexibility with task switching (Blakemore & Choudhury, 2006). The brain regions of the executive control network include the dorsolateral frontal and parietal neocortices (Seeley et al., 2007).

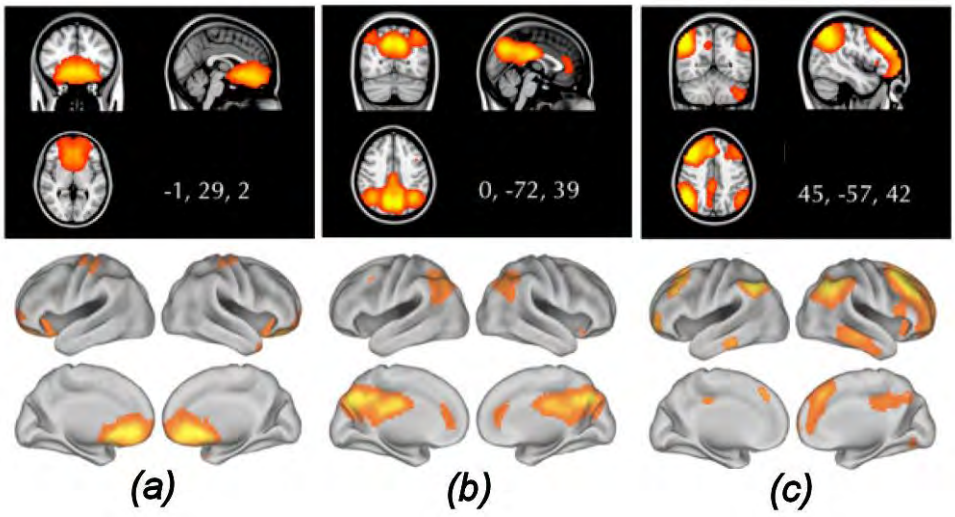

Figure 1: Standard brain views and surface plots of RSNs: (a) orbitofrontal DMN (b) posterior DMN, (c) executive control (figure adapted from Biswal et al., 2010).

The salience network (see Figure 2d) comprises of the dorsal anterior cingulate and orbital frontoinsula cortices. Its main function is to integrate external sensory information in order to regulate and manage neural responses (Seeley et al., 2007) and therefore is often linked to behavior performance. Recent studies have shown that the salience network is often activated in attention-demanding cognitive tasks and is largely accountable for error handling, by detecting the error and sending out a signal for behavioral adaption (Ham et al., 2013; Holroyd et al., 2004).

Dorsal attention and ventral attention (see Figure 2 e,f) are overlapping networks included in the broader category of the attention network (Ossandon et al., 2012; Vogel et al., 2012; Weissman et al., 2012; Ptak, 2012; Gao & Lin, 2012; Fox et al., 2006). The dorsal attention network is mainly responsible for the top-down orientation of attention; it includes the bilateral intraparietal sulcus and the junction of the superior and precentral frontal sulcus (Fox et al., 2006). The ventral attention network is responsible for reorienting attention in response to a salient sensory stimulus and is lateralized; it includes the right temporal-parietal junction and the right ventral frontal cortex (Fox et al., 2006).

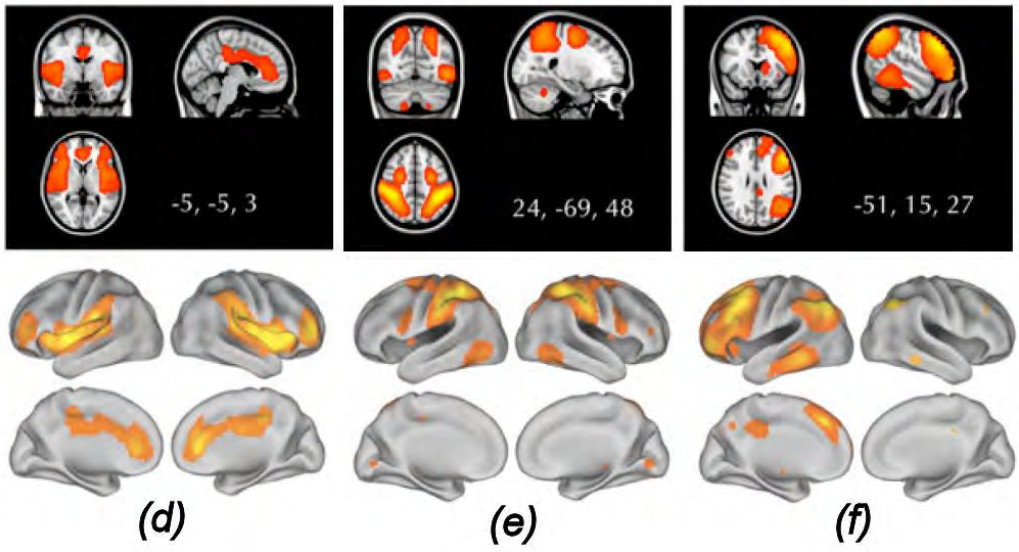

Figure 2: Standard brain views and surface plots of RSNs: (d) salience, (e) dorsal attention, (f) ventral attention (figure adapted from Biswal et al., 2010).

The visual, auditory and motor networks are responsible for sensorimotor functions (see Figure 3). The visual network includes the occipital cortex, temporal-occipital regions and the lingual gyrus. The auditory network includes a region of the superior temporal cortex, and the motor network includes the dorsal precentral gyrus and supplementary motor area (Husain & Schmidt, 2014; De Luca et al., 2006; Beckmann et al., 2005; Yeo et al., 2011). These networks are responsible for visual and auditory processing; language functioning; and motor control and coordination.

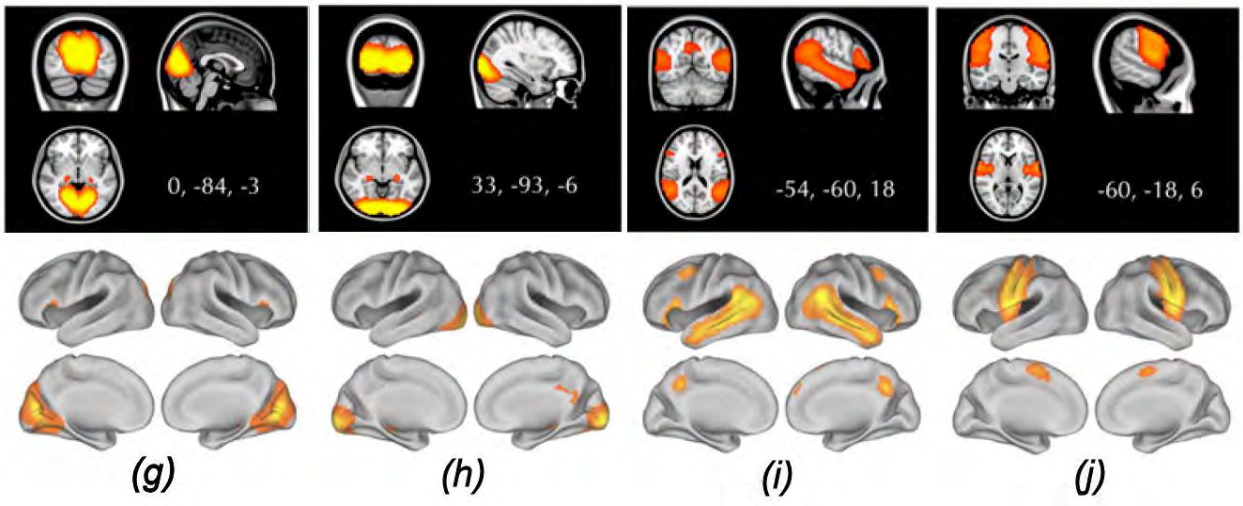

Figure 3: Standard brain views and surface plots of RSNs: (g) visual (lingual gyrus), (h) visual (occipital lobe), (i) motor, (j) auditory (figure adapted from Biswal et al., 2010).

A variety of analysis techniques can be used to quantify correlations between nodes in a network (Rogers et al., 2007); as such, numerous multivariate statistical approaches have been adapted and applied to analyze such datasets. The two methods typically used to extract information on the FC of RS-fMRI data are independent component analysis (ICA) and seed-based correlation analysis (SCA) (Lee et al., 2012; Cole et al., 2010; Long et al., 2008; Xiong et al., 1999; Biswal et al., 1995).

ICA is a standard algebraic technique that is used to separate an assortment of linear sources, based on their non-Gaussian distribution, into spatially independent patterns of activity (Calhoun et al., 2001; McKeown et al., 1998). It allows neuronal activity to be separated from other signal sources by decomposing the (flattened) 2D (time*voxel) data matrix into a set of time courses along with their associated spatial maps (Beckmann et al., 2005). The main assumption of ICA is that the underlying components are spatially independent and not merely uncorrelated (McKeown et al., 1998). It is a data-driven method that is sensitive to the model order selection (e.g. the number of independent components to decompose the data into) (Abou-Elseoud et al., 2010). However, it requires no prior hypothesis of spatial associations (besides independence) and can reveal inter-subject differences in the temporal dynamics, making it ideal for analyzing differences between groups of participants (Beckmann et al., 2005; Calhoun et al., 2001; McKeown et al., 1998).

On the other hand, SCA calculates the temporal cross correlation coefficients of the time series between a seed region and every other voxel in the brain. It is characterized as a model-driven analysis, as it requires a prior hypothesis by means of selecting a seed from which to extract the time series information (Cole et al., 2010). An advantage of SCA is the simplicity of interpretation, as the results indicate regions most strongly functionally connected to the seed (and assumes no inherent inter-network properties such as spatial independence).

We are of the view that each of ICA and SCA analyses has a role to play in interpreting fMRI data. In this study, we used each in the following manner: implementing ICA for conducting exploratory analyses, while performing SCA to directly investigate a hypothesis, such as the extent to which one region of interest is functionally connected to all other regions of the brain.

3. METHODOLOGY

3.1 STUDY COHORT

The participants for this study were a subset of HIV infected isiXhosa children from CHER trial who have been followed since birth at the Children's Infectious Diseases Clinical Research Unit (KID-CRU), Tygerberg Children's Hospital, in Cape Town, as well as uninfected children from the same isiXhosa community who were recruited as part of an interlinking vaccine trial (Madhi et al., 2010). The uninfected children consisted of unexposed children (born from uninfected mothers) and exposed children (born from HIV infected mothers and who were therefore also exposed to HAART in utero).

The CHER trial investigated different ART strategies in infants and children from resource limited settings over a 5-year period (Cotton et al., 2013; Violari et al., 2008), while a separate sub-study performed at the KID-CRU investigated neurodevelopment in the CHER children residing in Cape Town and uninfected children from the above-mentioned interlinking vaccine trial. As part of the present study, these children are being followed for a further 4 years with neuroimaging and neurocognitive testing at 5, 7 and 9 years (with scanning currently underway at 9 years). In this thesis, results are reported from functional neuroimaging data acquired at age 7 years.

For the CHER trial, HIV infected pregnant women were recruited from the public PMTCT programme. The drugs administered included: Zidovudine (ZDV, AZT, Retrovir) for 34 weeks to pregnant mothers and for 7 days to newborns; as well as a single dose of Nevirapine (NVP, Viramune) to the mothers during labor and to all infants shortly after birth (Cotton et al., 2013). To confirm HIV infection, a positive polymerase-chain-reaction (PCR) test was administered to both infected and uninfected exposed children. PCR measures the HIV-1 DNA and PVL in a subject and a test value of HIV-1 RNA > 1000 copies per milliliter was necessary for the child to be confirmed HIV positive. Available clinical measures for the HIV infected children include CD4 count, CD4 percent (CD4%), CD4/CD8, and PVL at time of enrollment; along with CD4 count and CD4% at the time of neuroimaging.

The HIV infected CHER children were enrolled between 6–12 weeks of age and were randomly distributed into the following three treatment arms: a) ART-Def (ART deferred until CD4% < 25% in first year or CD4% < 20% thereafter, or if clinical disease progression criteria

presented), b) ART-40W (ART initiated immediately and interrupted after 40 weeks), and c) ART-96W (ART initiated immediately and interrupted after 96 weeks). For the ART-Def group, once ART was started, it was given continuously. For the ART-40W and ART-96W, a clinical criterion was used to determine when to restart ART (i.e. at the time of interruption or at a later date), once restarted, the child remained on ART. All of the children included in the study had a CD4% $\geq$ 25% at enrollment and they completed comprehensive clinical and immunological follow-up until the age of 5 years as part of the original CHER trial. Thereafter, the follow-ups continued as part of the current study. At the time of scan, all HIV infected children were receiving HAART. The ART regimens for all treatment arms consisted of ZDV + Lamivudine (3TC, Epivir) + Lopinavir+Ritonavir (LPV/r, Kaletra).

3.2 MRI ACQUSITION

100 isiXhosa children (mean age$\pm$sd = 7.2 ± 0.14 years; 50 males) received high-resolution structural and RS functional neuroimaging on the 3T Allegra (Siemens, Erlangen, Germany) MRI located at the Cape Universities Brain Imaging Centre (CUBIC) adjacent to Tygerberg Hospital. All protocols were approved by the Faculty of Health Sciences Human Research Ethics Committees of both the Universities of Cape Town and Stellenbosch. All parents provided written informed consent and all children provided oral assent, which included screening for suitability using a simulation scanner. Children were not sedated or anesthetized and were able to request that the scan be stopped at any point through use of a squeeze ball in the scanner.

T1-weighted structural images were acquired in the sagittal slices using a motion navigated (Tisdall et al., 2009) multiecho magnetization prepared rapid gradient echo (MEMPRAGE) sequence (Van der Kouwe et al., 2008) with TR 2530 ms, TEs (1.53, 3.19, 4.86, 6.53)ms, inversion time (TI) 1160 ms, flip angle 7 degrees, resolution 1.3 x 1 x 1 mm^3, field of view (FOV) 224 x 224 x 144mm^3. RS-fMRI scan were also acquired: 180 volumes sensitive to BOLD contrast were acquired with a interleaved multi-slice 2D gradient echo, echoplanar imaging (EPI) sequence, voxel size 3.4 x 3.4 x 5 mm^3, 33 interleaved slices acquired from bottom up, 1 mm gap, TR/TE 2000/30 ms, flip angle 77 degrees, FOV 220 x 220 x 164 mm^3, matrix size 64 x 64).

3.3 EXCLUSION CRITERIA

A number of exclusion criteria were applied to the acquired data for quality assurance purposes: having incomplete structural or RS-FMRI data; data with poor image quality (for example, data demonstrating poor registration to the Talairach template or visible artifacts, such as signal dropout); and exhibiting motion more than 3mm translation or 3° rotation in any direction (3 translation and 3 rotational degrees of freedom). For subjects included in the study, further motion considerations were applied during the functional data preprocessing and main analyses, as described below.

3.4 IMAGE PROCESSING

All analyses were carried out using a combination of in-house scripts developed by the author and tools available in standard software packages, namely the FMRIB Software Library (FSL) (Jenkinson et al., 2012; Woolrich et al., 2009; Smith et al., 2004) and the Analysis of Functional Neuroimages (AFNI) toolbox (Cox 1996).

3.4.1 PREPROCESSING

The RS-fMRI data were preprocessed prior to statistical and connectivity analyses. Structural images were skull-stripped and used for alignment purposes during this process. Preprocessing was performed using AFNI software package by constructing and customizing a pipeline using *afni_proc.py* (Figure 4).

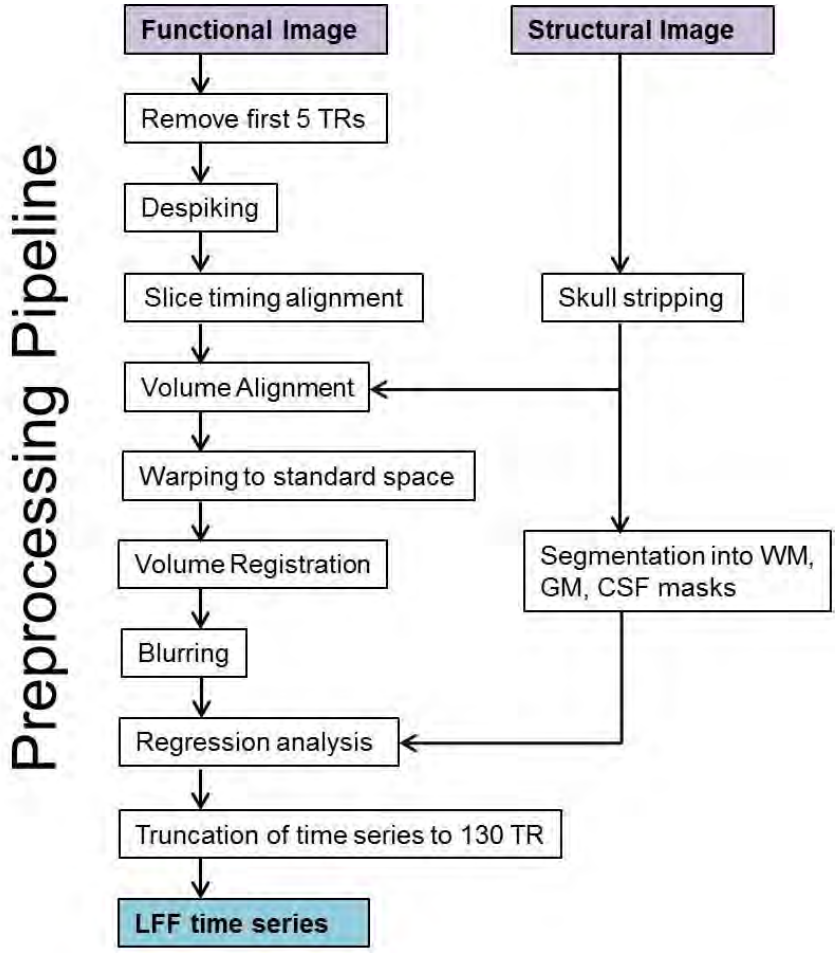

Figure 4: Preprocessing pipeline of all participants' datasets.

The first 5 volumes of the RS-fMRI were removed, as the proton magnetization requires a few seconds to reach a steady state. Despiking was applied to remove large, sudden outliers from each voxel's time series (e.g. due to motion effects, speckle noise and random noise). Slice timing alignment was used to adjust the voxels time series in the functional image to ensure that separate slices were aligned to the same temporal origin.

Volume alignment of the functional images to the skull stripped structural image was performed, resulting in EPI-distortion correction within the fMRI time series. The functional images were then warped into 3mm standard space using the Talairach transformation. For this study, nonlinear warping was performed to map each participant's functional data to a standard 3mm Talairach template. Volume registration was applied in 6 degrees of freedom (DOF), resulting in motion correction within the fMRI series.

The data were spatially smoothed using a 6mm full width at half maximum (FWHM) Gaussian blur and three brain tissue masks (WM, GM, CSF) were created from segmenting the structural image. Lastly, eroded CSF and WM average time series along with their derivatives were regressed from the volumes as they contain a record of motion. A bandpass filter between 0.01-0.1Hz was then used to extract the LFF time series of interest in the RS-fMRI data, using a demeaned derivative of the motion confound - in order to regress motion and the derivative of motion.

3.4.2 MOTION PARAMETERS

While the preprocessing steps aim to reduce the effects of noise and motion artifacts, there may still be some potential non-neurological signals (e.g. respiratory and cardiac signals, as well as motion residual in the data. The participant's motion and its influence on the dataset was a large concern in this study as MRI analysis is extremely sensitive to movements and children often struggle to keep still during the scan. Therefore, several steps were taken to account for potential motion artifacts in order to minimize their impact on the results.

The first round of motion correction was implemented during the volume registration stage of the preprocessing pipeline (explained above in Section 3.4.1), whereby each fMRI volume was registered to the base volume. By default the reference base for volume registration was the first volume of the dataset. This produced a motion file containing a record of each subject's estimated integral movement (as calculated by the 6 DOF rigid-body registration process) for the duration of the scan.

As a criterion for inclusion, each subject was required to have at least 130 time points with motion below the threshold of 3 mm translation or 3° rotation, as quantified by the 6 DOF parameters. If this criterion was not met when using the default first time point as a reference base, then the base was changed to see whether a later volume provided a better reference to subsequent volumes (i.e. for a period of 130 time points with sub-threshold motion); this would be the case if, for example, there was an early instance of motion and only sub-threshold motion thereafter.

To find a suitable new base, the differential motion between successive volumes was estimated from the registration file, and then the integral amount of motion between all volumes and the new reference volume was generated. If the new reference resulted in having at least 130 consecutive volumes satisfying the motion criterion, then the subject's data (for that interval of

low-motion volumes) was included. For consistency, all included subjects' time series were truncated to 130 time points.

Although individual-level motion correction using 6 DOF was implemented during volume registration, the application of the motion threshold criterion does not sufficiently bypass the need for group-level correction in the dataset (Yan et al., 2013). Therefore, a representative motion parameter was included as a confound in the model design for all main analyses that were performed (see Section 3.5). This parameter was estimated for each participant as follows: first, the voxel-wise framewise displacement (VWFD) was calculated for each volume in the time series from the three translational degrees of freedom (recorded in the time series registration file) (Yan et al., 2013); then, VWFD values were averaged together to provide the motion confound for each participant to be used in the models described below.

Furthermore, we also used the average VWFD values to investigate whether subject motion differed significantly across groups, in order to ensure that it was not a driver in the final results of the main analyses. As with other group characteristics, a two sample T-test was performed between HIV infected and uninfected participants and between unexposed and exposed uninfected participants. Analysis of variance (ANOVA) was implemented for a comparison across the 3 arms of the infected groups.

3.4.3 MODEL DESIGN

The main data analyses conducted in this study (see Section 3.5) were performed using general linear models (GLMs) to investigate the association between FC and various HIV related features, while simultaneously controlling for additional sources of variance. Each model was implemented by setting up a design matrix using FSL's *GLM* tool (Smith et al., 2004; Woolrich et al., 2009; Jenkinson et al., 2012). The design matrix enables the investigation for significant relations between observations and a predictor of interest while controlling for confounds. In experimental designs, one needs to balance the inclusion of confounds with the statistical power of the dataset. This generally leads to the aim of selecting only confounds which have significant effects on the modeled data.

Based on previous literature and the sample characteristics of this dataset, three potential confounding variables were identified: subject sex, age at scan and motion (quantified by the VWFD values). The efficacy of including age at scan and sex (F=1, M=0) confounds was

investigated using several procedures to identify the impact that each of these confounds had on the dataset. Each variable in the model was standardized.

First, we examined the individual effects of each of the three potential confounds on the connectivity data. The preliminary GLMs were set up to include one predictor with contrasts to examine group level differences between the infected and uninfected children, along with supplementary contrasts to test the positive and negative effect that the confound had on the dataset. Each RSN of interest obtained from FSL's MELODIC (Multivariate Exploratory Linear Optimized Decomposition into Independent Components) function was tested; FSL's *dual_regression* and *randomise* functions were used to produce the probability and test statistic maps, and AFNI's *AlphaSim* tool was used to implement voxel-wise thresholding at a $p<0.05$. The resulting *Z*-score group-level difference maps were examined along with the effect maps to establish the extent of impact that each confound was having on the resulting maps.

Two supplementary tests were used to further verify which confounds were to be included. A two sample T-test and ANOVA were used to investigate whether there were significant group differences in the confound values (e.g., did one group have more motion than the other); and the variance inflation factor (VIF) was also calculated for the model variables. The VIF indicates the collinearity of model variables. Generally, a VIF < 5 is taken to indicate that collinearity among variables is sufficiently low in a model (Hair et al., 1995; Neter et al., 1989).

Using these methods, the impact of each confounder on the data was determined and provided a good indication and motivation as to which confounds needed to be included as regressors in the GLM for the final model design. It was determined that sex and motion needed to be included in the model design while age did not impact the data, presumable due to the narrow age range of participants.

3.5 DATA ANALYSIS

The preprocessed LFF time series of the participants were utilized in three main analyses to investigate the association of FC with HIV infection and treatment. In the primary analysis, group comparisons were made for both within-network and network-to-whole-brain connectivity effects. Two follow-up investigations were of factors within each of the main groups. Within the infected group we examined the association of continuous clinical measures with FC changes. Finally, we performed a follow-up investigation of subcategories within the uninfected group. Therefore, the overall structure of the analyses in this study was as follows:

1) Group differences in FC: infected children on HAART vs. uninfected children
    A) within functional RSNs using ICA
    B) across the whole-brain connectivity using SCA
2) FC association with clinical measures in HIV infected children on HAART: correlation with the CD4/CD8 at time of enrollment within RSNs using ICA
3) Group differences in FC: unexposed vs. exposed uninfected children
    A) within functional RSNs using ICA
    B) across the whole-brain connectivity using SCA

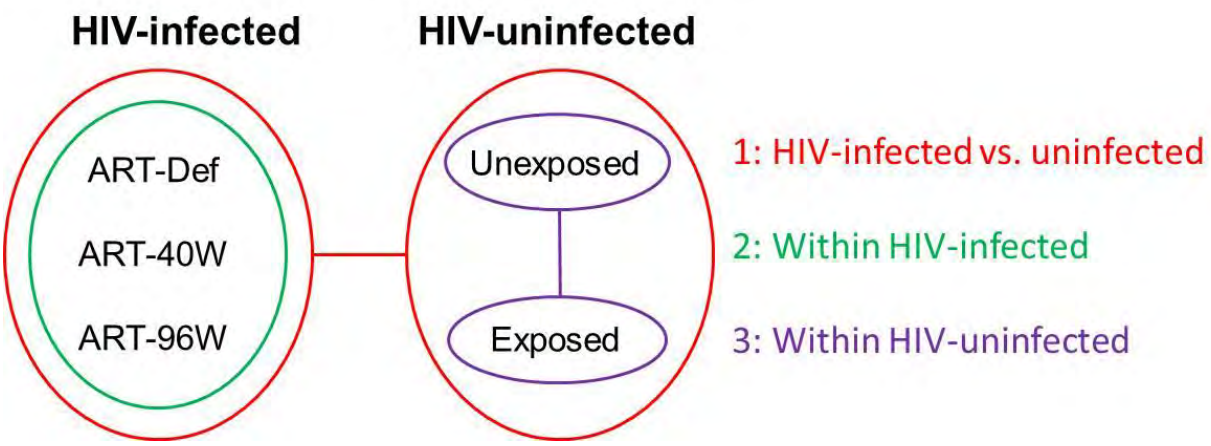

Figure 5: Graphical representation of the three main analyses conducted in this study. Analysis 1 (infected vs. uninfected) constitutes the main investigation of this study. Exploratory Analyses 2 and 3 contributed to an understanding of factors within each of the main groups and to the results of Analysis 1.

3.5.1 HIV INFECTED VS. UNINFECTED CHILDREN, USING ICA

All subjects' datasets were placed into two groups: infected (including all three treatment arms) and uninfected (including exposed and unexposed). A schematic of the steps of this analysis is shown in Figure 6. First, group independent component analysis (group-ICA) was performed using FSL's MELODIC function on the whole sample (i.e., HIV infected and uninfected children). MELODIC spatially flattens and concatenates all the individual datasets into a single, 2D dataset and then performs ICA to decompose it into a chosen number of spatially (statistically) independent components (ICs), each with an associated time course. For this study, MELODIC was set to decompose the resting state data into 20 ICs, a standard number in RS-fMRI studies

of similar group size (Smith et al., 2009). Each IC map is comprised of *Z*-scores that represent the degree of correlation that each voxel has with the IC's associated time course. High *Z*-values imply a high degree of correlation between the voxel and the associated IC's time course.

Importantly, in RS-fMRI studies several of the ICs reflect functional networks, referred to as RSNs: other components, as is standard, can be associated with, for example, noise and registration features. The RSNs of interest were established by visual inspection and by quantitative correlation to the well-established RSN templates produced by the FCP (Biswal et al., 2010), as well as those of two previous pediatric RS-fMRI studies (de Bie et al., 2012; Thomason et al., 2011). In this study, 9 ICs were identified as corresponding to RSNs, and these were retained for further analysis. The remaining ICs were not considered further. Within the retained ICs, regions of high FC within the network were identified by thresholding the *Z*-score maps at $Z>3$ (equivalent to a $p<0.001$), and binarized to form RSN spatial masks.

Using the full group-ICA time series as a regressor and the participants LFF time series, the subject-specific spatial connectivity maps were obtained for each RSN using FSL's *dual_regression* function, by means of back projection. The subject-specific spatial connectivity maps, along with a group model design matrix and the RSN spatial masks, were input into FSL's *randomise* function, in order to perform nonparametric permutation inference by means of cross-subject voxel-wise analysis (i.e., between group voxel-wise analysis). The design matrix was created using FSL's *GLM* tool and contained all the participants along with their respective group assignments and their confound values for sex and motion. The contrasts were set up to perform a 2 sample t-test based on the main effects of diagnosis (i.e., uninfected>infected and infected>uninfected), as well as to generate mean effect maps for each group (i.e., infected and uninfected groups). For each contrast, 5000 Monte Carlo permutations were run with voxel-wise thresholding based on the null distribution of the max (across the image) voxel-wise test statistic. The end results were voxel-wise test-statistic and probability maps for each modeled contrast.

In order to account for the large number of multiple comparisons involved in the *randomise* results (due to the large number of brain voxels), AFNI's *AlphaSim* tool was used to find the significant clusters from the group level difference maps (Liu et al., 2013; Qui et al., 2011; Zou et al., 2009; Long et al., 2008; Wang et al., 2007; Wang et al., 2006), while controlling for

multiple comparisons by means of Monte Carlo simulations. The simulations are based on the combination of voxel probability thresholding and minimum cluster size thresholding, with respect to the number of voxels within each RSN spatial mask. 5000 permutations were run for each RSN using the face-wise criterion for neighboring voxels (i.e., each voxel has 6 neighbors). The overall significance level was set to $\alpha < 0.05$ and the individual voxel-wise significance level was determined using Bonferroni correction of α/N where N is the number of simultaneous inferences, in this case being the 9 RSNs of interest. The RSN spatial masks were used to obtain the relevant voxel count for each RSN. The estimated inherent smoothness of noise structures across the brain in the respective RSN masks were obtained by calculating the FWHM values in three directions (x,y,z) for each participant and then averaging across all participants to obtain the mean FWHM value in the individual x, y, and z direction. *AlphaSim* provided the minimum size for a cluster to be considered significant, based on the above thresholds.

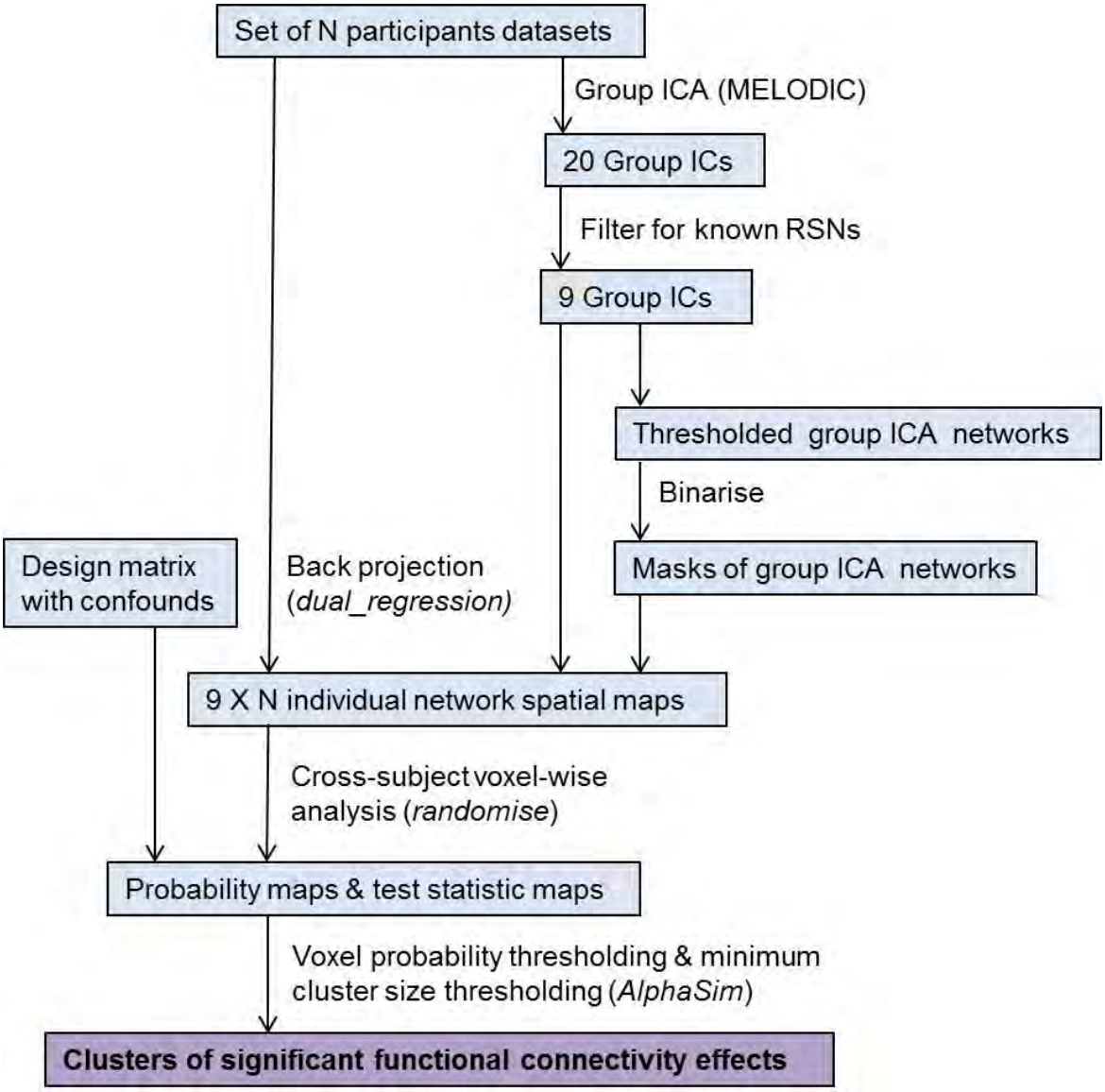

Figure 6: Pipeline of analysis: HIV infected vs. uninfected children, using ICA.

3.5.2 HIV INFECTED VS. UNINFECTED CHILDREN, USING SCA

Whole-brain, FC differences between the infected and uninfected children (the latter including all three treatment arms) were investigated with SCA using AFNI. A schematic of the steps of this analysis is shown in Figure 7. Spherical seeds, (5mm radius and restricted by the network boundaries), were centered upon the global peak value of the *Z*-score map from each RSN retained from group-ICA. In RSNs with large anteroposterior spread, a second seed was also chosen at an extreme anteroposterior position compared to the initial seed, in order to explore

potentially different features of the network. Lateral spread was not examined, as left-right homotopy typically leads to high correlation along this axis.

For each subject, the mean time series within the spherical seeds was used as a reference for whole-brain connectivity analysis, meaning the reference time series was cross-correlated with every other voxel within the brain. Correlation values were Fisher transformed to *Z*-scores, forming an SCA map. The resulting *Z*-score maps were then concatenated across all participants to create a whole-brain voxel-wise RSFC map of covariance with each seed.

The concatenated SCA maps were utilized in a similar analysis as the subject-specific spatial connectivity maps produced by *dual_regression* in the previous analysis. FSL's *randomise* function was used to perform voxel-wise between group comparisons, using the same design matrix as described previously. Using AFNI's *AlphaSim* tool, correction for multiple comparisons were implemented in a similar fashion as described previously with a few different parameters. In this case, the voxel-wise significance level was set based on the number of seeds (N = 16). Also, the whole-brain mask was used to obtain the relevant voxel count and the estimated inherent smoothness of noise structures across the brain from the FWHM values in the individual x, y, and z directions. *AlphaSim* provided the minimum cluster size necessary for the extracted group-level differences to be considered significant – based on the parameters stipulated above.

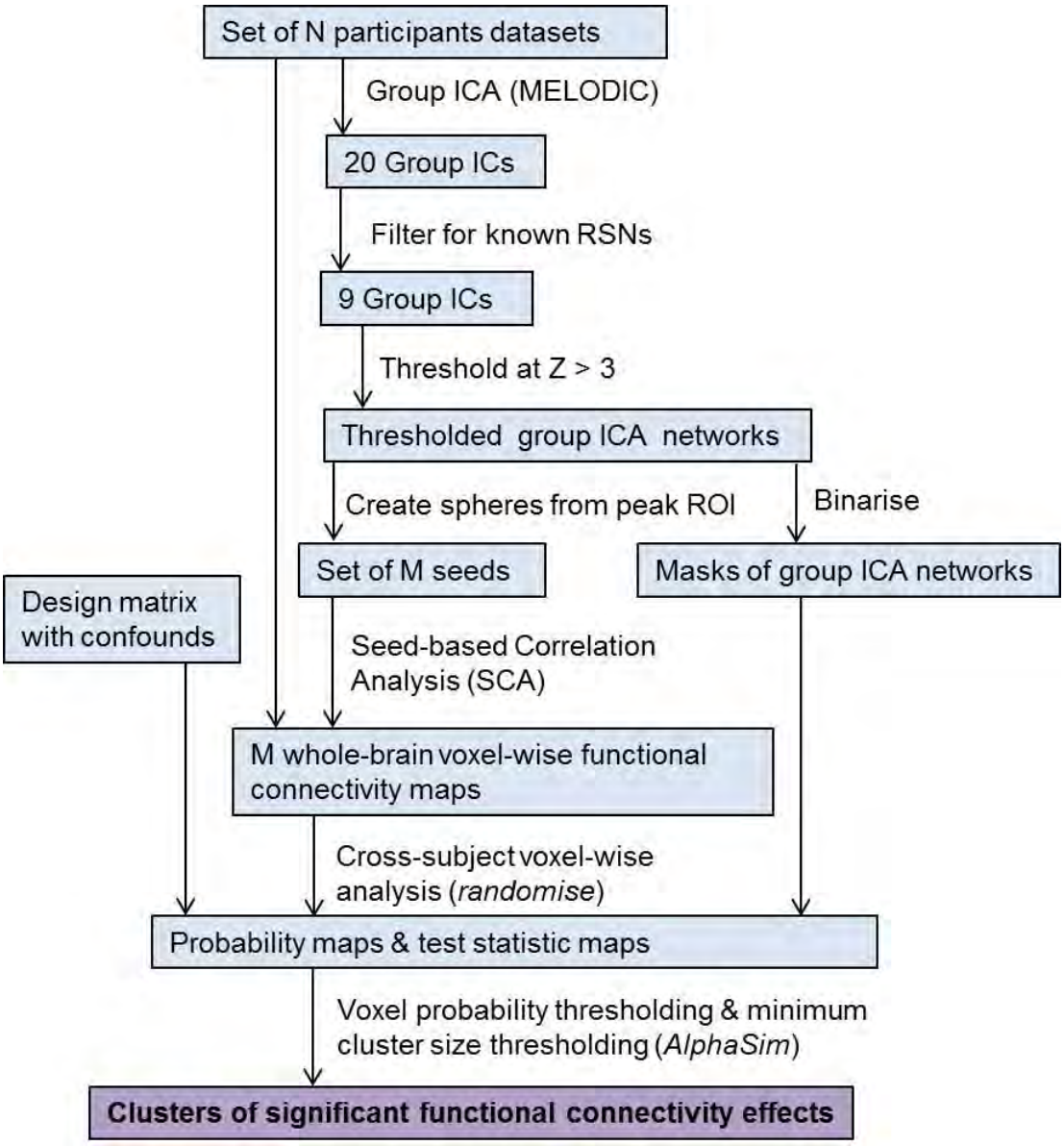

Figure 7: Pipeline of analysis: HIV infected vs. uninfected children, using SCA.

3.5.3 ASSOCIATIONS OF CONNECTIVITY AND CLINICAL MEASURES AMONG INFECTED CHILDREN

Within the HIV infected group, associations between the clinical measure CD4/CD8 obtained at time of enrollment and the RSFC values within RSN maps were examined. The design matrix contained the same set of confounds retained in the previous analyses, namely subject motion and sex. The contrasts were set to test for the positive and negative linear relationship of the CD4/CD8 with the FC values within each of the thresholded RSNs.

FSL's *dual_regression* and *randomise* functions, along with AFNI's *AlphaSim* tool, were implemented in a similar manner to that described previously. Since a continuous variable was being investigated in this case, the *randomise* procedure was performed with a GLM instead of a two-sample t-test, which had been used in the group comparison.

The resulting test statistic maps were converted to correlation maps in order to illustrate the extent of correlation between the clinical measure of interest and any brain regions found to have a significant association to the clinical measure. Correlation graphs were also produced for any clusters found by plotting the clinical measure against the average Z-score over the region extracted for each participant.

3.5.4 WITHIN UNINFECTED, EXPOSED VS. UNEXPOSED, USING ICA AND SCA

As a final exploratory analysis, we investigated FC differences within the uninfected group using first ICA and then SCA. The same ICA and SCA pipelines were followed as for the group differences (i.e. infected vs. uninfected children), except that in this case, the groups consisted of unexposed vs. exposed uninfected participants.

4. RESULTS

4.1 SAMPLE DEMOGRAPHICS

The final sample consisted of 45 participants, including 27 HIV infected subjects (18 female, 9 male) and 18 uninfected subjects (11 female, 7 male). The demographics and characteristics for the infected and uninfected children are presented in *Table 1*. Neither subject age, sex, birth weight nor estimated motion during scanning were significantly different (p<0.05) between the infected and uninfected children.

Table 1: Sample demographics of the infected and uninfected subjects. Values indicated are mean $\pm$ sd. Motion is calculated using the average VWFD estimate for each participant.

	Infected group	**Uninfected group**	t / χ^2	p
N	27	18		
Age (years)	7.20 $\pm$ 0.08	7.20 $\pm$ 0.16	-0.01	0.994
Sex (%M)	33.33%	38.88%	0.15	0.703
Birth weight (*g*)	3077.41$\pm$ 528.48	3078.89$\pm$ 492.60	0.01	0.993
Motion (mm)	0.12 $\pm$ 0.70	0.13 $\pm$ 0.96	0.52	0.608

The sample demographics, as well as the clinical measures at enrollment and at time of scan, for the three treatment arms within the infected group are presented in Table 2. There were no significant (p<0.05) between group differences in demographics or clinical measures (either at enrollment or at time of scanning), and the treatment arms differed only in the age of ART initiation, as per study design. Within each treatment arm, the distributions of the clinical variables exhibited large standard deviations. For all treatment arms, the CD4 count was higher at enrollment than at time of scan. Unfortunately, the CD8 count was not measured at the time of scanning, and therefore the CD8 count and CD4/CD8 values cannot be compared between enrollment and time of scan.

Table 2: Sample demographics and clinical measures for the three treatment arms within the HIV infected group. Values indicated are mean±sd. Motion is calculated using the average VWFD estimate for each participant. [a]CD8 count missing for one participant in the ART-Def group.

	ART-Def	ART-40W	ART-96W	F / χ^2	p
N	9	11	7		
Age (years)	7.18 ± 0.06	7.25 ± 0.07	7.17 ± 0.11	2.53	0.101
Sex (%M)	22.22%	18.18%	71.43%	7.56	0.272
Birth weight (g)	2882.22± 570.02	3216.36± 585.29	3110.00± 335.11	1.01	0.380
Age of ART initiation (weeks)	36.94±22.18	8.47±1.26	11.37±6.74	12.85	**0.001**
Motion (mm)	0.13 ± 0.08	0.09 ± 0.05	0.15 ± 0.07	1.94	0.166
Enrollment					
CD4 count	1704.89 ± 484.49	2164.91 ± 1042.07	1872.86 ± 505.04	0.91	0.415
CD4%	35.24 ± 6.91	36.05 ±10.46	28.81 ± 6.23	1.74	0.197
CD8[a]	1389.67±482.75	1697.55 ± 1478.46	2244.86 ±1145.43	1.05	0.368
CD4/CD8[a]	1.37 ± 0.63	1.81 ±1.18	1.08 ± 0.68	1.34	0.281
Scan					
CD4 count	1257.22 ± 448.48	1101.09 ± 236.35	1367.00 ± 528.26	1.00	0.384
CD4%	36.91 ± 5.14	34.17 ± 6.80	37.00 ± 6.83	0.63	0.539

The uninfected participants in this study consist of both HIV exposed and unexposed children. The sample demographics of these sub-groups are presented below in Table 3. There were no significant differences in subject age, sex, birth weight or motion during scanning between exposed and unexposed children.

Table 3: Sample demographics for unexposed and exposed uninfected subjects Values indicated are mean±sd. Motion is calculated using the average VWFD estimate for each participant.

	Unexposed uninfected	Exposed uninfected	t / χ^2	p
N	10	8		
Age (years)	7.21± 0.20	7.19 ± 0.08	-0.34	0.741
Sex (%M)	30%	50%	3.38	0.066
Birth weight (kg)	3064.00± 351.95	3097.50± 655.23	0.14	0.892
Motion (mm)	0.18 ± 0.11	0.09 ± 0.06	2.11	0.061

Due to the exclusion criteria applied, a number of participants could not be included in the study, as summarized in Table 4. A total of 33 participants had unsuccessful or incomplete scans due to claustrophobia, restlessness or crying during the scanning session. Furthermore, three datasets did not register adequately to the Talairach template and six contained significant ghosting artifacts from the acquisition. Finally, 13 participants did not meet the motion criteria (requiring 130 consecutive TRs with less than 3mm translational or 3° rotational) and therefore were excluded from the study.

Table 4: Summary of number of participants excluded due to various exclusion criteria.

Exclusion criteria	Number of participants excluded
Unsuccessful/incomplete scans	33
Registration issues	3
Image artifacts	6
Excess motion	13
TOTAL EXCLUDED	**55**

4.2 RESTING STATE NETWORKS

Twenty components were extracted with MELODIC from the group-ICA analysis, represented as whole brain *Z*-score maps. Each component was visually inspected and quantitatively compared to the FCP template maps (Biswal et al., 2010) using the 3dMatch function from

FATCAT (Functional And Tractographic Connectivity Analysis Toolbox) (Taylor & Saad, 2013). A total of 9 RSNs of interest were identified as standard functional networks (Table 5). As is standard in ICA, the remaining eleven networks did not represent functional networks, but influences such as CSF, alignment artifacts and noise. The RSNs were thresholded at *Z>3* and then binarized to form network masks (Figure 8).

Table 5: List of identified RSNs along with the network name, abbreviation, and component number (IC#) corresponding to this study and to the FCP template.

Network Name	**Abbreviation**	**IC#**	
		here	**FCP**
Visual (lingual gyrus)	vis1	00	01
Visual (occipital lobe)	vis2	02	02
Posterior default mode	pDMN	04	06
Default mode	DMN	07	05
Dorsal attention	datt	05	09
Salience	sal	06	16
Auditory	aud	08	18
Motor	mot	10	19
Executive control	exe	12	11

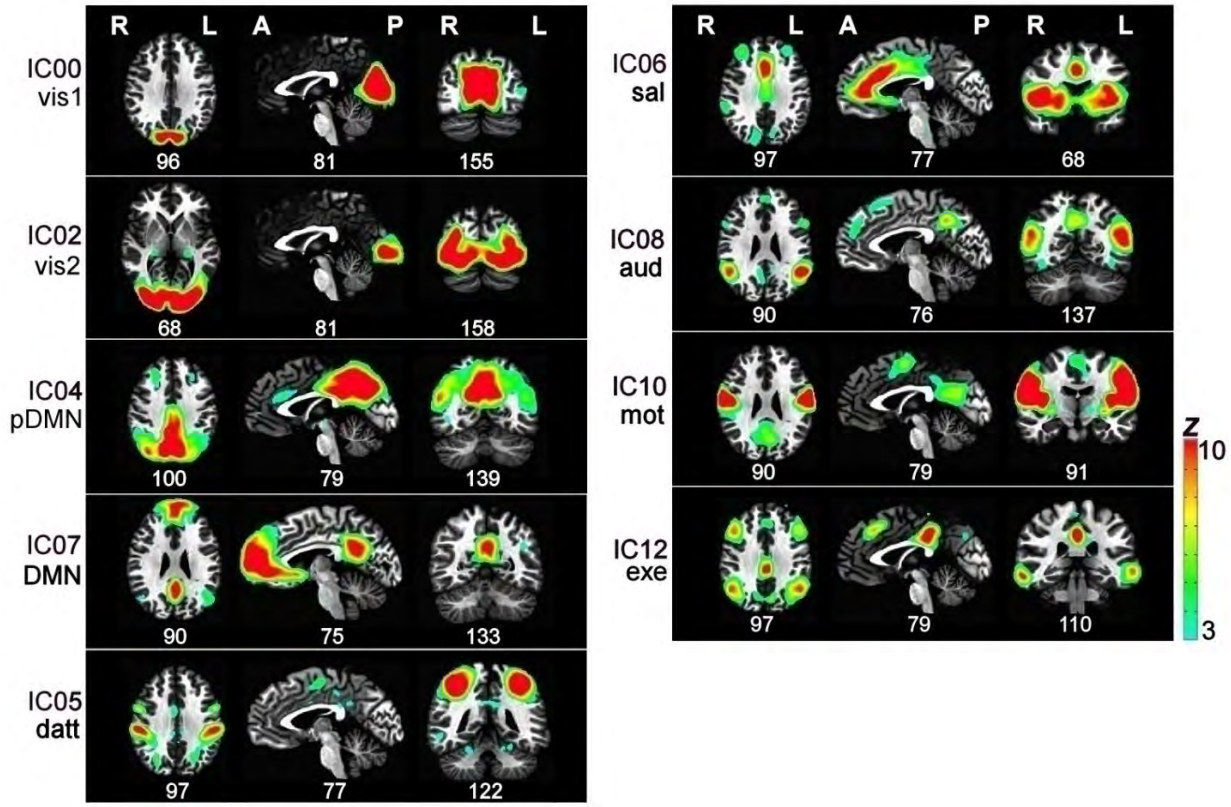

Figure 8: *Z*-score maps (*Z*>3) extracted from group-ICA, representing the nine RSNs of interest: visual lingual gyrus (vis1); visual occipital lobe (vis2); posterior default mode network (pDMN); default mode network (DMN); dorsal attention (datt); salience (sal); auditory (aud); motor (mot); and the executive control (exe) networks.

4.3 MODEL DESIGN

When examining the impact of each potential confounder (sex, motion and age) on group level differences between the infected and uninfected children, we found that both sex and motion confounds significantly changed the group level differences (at a voxel-wise threshold of $p<0.05$) in two ICs extracted from ICA. Age did not affect the outcome; this was expected as age was very similar across the subjects. From the participants used in the main analyses, 96% were scanned within 2 months of their 7th birthday, leaving only two participants that were scanned within 3 – 6 months of their birthday. Therefore, only the sex and motion confounder were added to the design matrix for all analyses performed. In calculating the VIF for quantifying collinearity in the model variables, it was found that the maximum value in any model was 4.2,

which is below the standard threshold value of 5 (Hair et al al. 1995; Neter et al., 1989) and therefore the models were implemented as described above.

4.4 DATA ANALYSIS

4.4.1 HIV INFECTED VS. UNINFECTED, USING ICA

Each RSN identified from group-ICA was used to compute group level differences between infected and uninfected participants by performing voxel-wise analyses across subjects, using FSL's *dual_regression* and *randomise* tools. The average FWHM values across all networks ranged between 8.1-9.8 mm. The minimum cluster size for significant group differences ranged between 24 and 31 voxels (i.e., 648 and 837 mm^3). No significant clusters of FC differences were found between the infected and uninfected groups in any of the RSNs.

4.4.2 HIV INFECTED VS. UNINFECTED, USING SCA

In order to perform SCA, a total of 16 spherical seeds (5 mm radius) were created at peak values across the 9 RSN maps (one global peak per network, and in some cases one or more additional local peaks). Locations of the seeds are summarized in Table 6*;* including the peak coordinate values in Talairach space and the anatomical location of the seed (using the Talairach atlas provided by AFNI).

Table 6: Seed locations for SCA. Coordinate values are provided, along with the anatomical locations of the seeds.

Seed #	Network	Peak coordinate in Talairach space (mm)			Anatomic location
		x	y	z	
1	Visual (lingual gyrus)	-1.5	76.5	11.5	R cuneus
2	Visual (occipital lobe)	-31.5	85.5	5.5	R middle occipital gyrus
3	Posterior default mode	-4.5	67.5	32.5	R cuneus
4		-4.5	37.5	26.5	R cingulate gyrus
5	Dorsal attention	-37.5	37.5	44.5	R inferior parietal lobule
6		28.5	13.5	56.5	L precentral gyrus
7	Salience	37.5	-7.5	2.5	L insula
8		-1.5	-34.5	14.5	R anterior cingulate
9	Default mode	1.5	-61.5	5.5	L medial frontal gyrus
10		1.5	46.5	29.5	L cingulate gyrus
11	Auditory	-49.5	28.5	2.5	R superior temporal gyrus
12	Motor	-55.5	10.5	17.5	R postcentral gyrus
13	Executive control	-40.5	55.5	41.5	R inferior parietal lobule
14		-1.5	31.5	38.5	R cingulate gyrus
15		58.5	40.5	-3.5	L middle temporal gyrus
16		-40.5	-16.5	38.5	R middle frontal gyrus

The required *AlphaSim* parameters included an overall significance level of $\alpha<0.05$ and an individual voxel-wise significance level of $p<0.05$, corrected for multiple comparisons of 16 seeds, and an average FWHM value of 8.66mm for the whole-brain. The minimum cluster size for significance at the above-defined levels within the investigated whole-brain mask was 44 voxels (1188mm^3).

The voxel-wise two-sample t-test examining FC between the seed regions and the whole brain revealed significant clusters of group level differences in two regions: the left middle frontal gyrus (seed in the left cingulate gyrus of the DMN; Figure 9a), and the right supramarginal gyrus (seed in the right middle frontal gyrus of the executive control network; see Figure 9b). Clusters and peak locations are shown in Table 7. In both cases, the infected children showed decreased connectivity compared to the uninfected children.

Table 7: Clusters showing greater FC in uninfected children compared to infected children. For each cluster, the coordinates of the peak difference are shown, as well as the anatomical location and size (in voxels).

Seed information			Clusters of FC difference (uninfected > infected)				
Seed #	Network	Seed location	Size (voxels)	Peak coordinate in Talairach space (mm)			Anatomical location
				x	y	z	
10	Default mode	L cingulate gyrus	55	31.5	-34.5	-12.5	L middle frontal gyrus
16	Executive control	R middle frontal gyrus	49	-49.5	46.5	32.5	R supramarginal gyrus

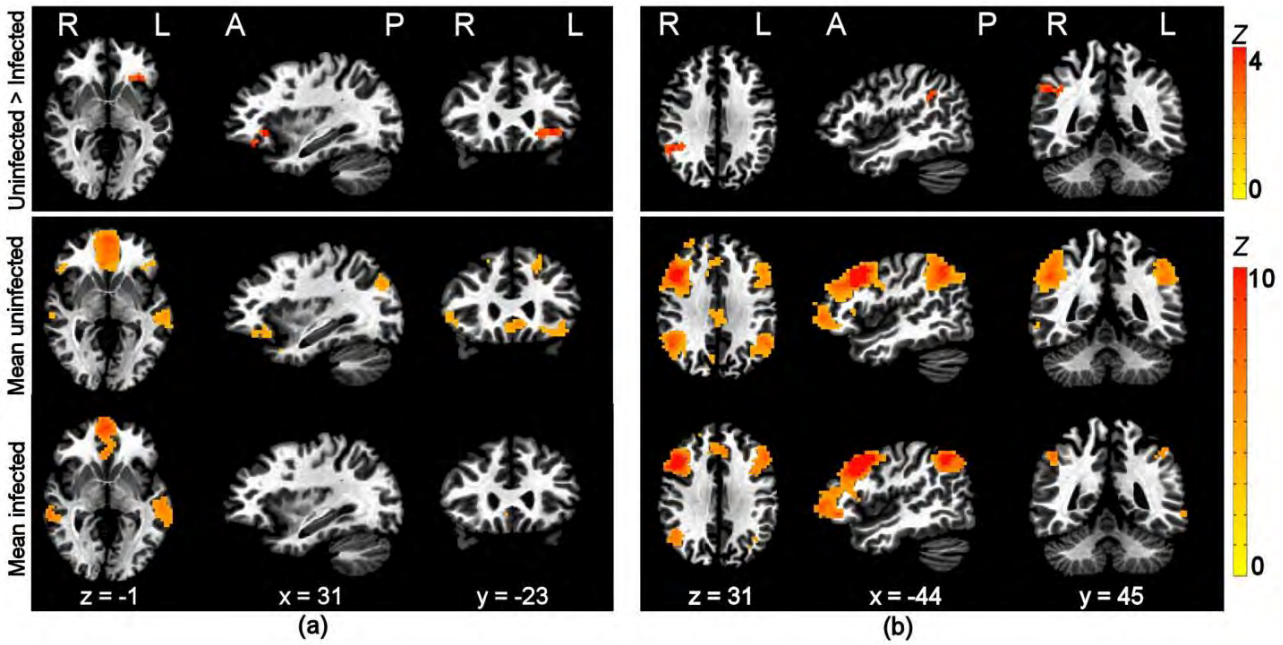

Figure 9: Regions showing differences in connectivity between infected and uninfected children with a seed in the a) default mode (left cingulate gyrus) and b) executive control (right middle frontal gyrus) networks. The top panel shows regions where connectivity differed in the a) left middle frontal gyrus and b) right supramarginal gyrus at a threshold of $p<0.05$ (corrected for multiple comparisons of 16 seeds). The middle and lower panels show the mean connectivity maps to the seed for the uninfected and infected children, respectively. The slice numbers in Talairach space are shown at the base of each column.

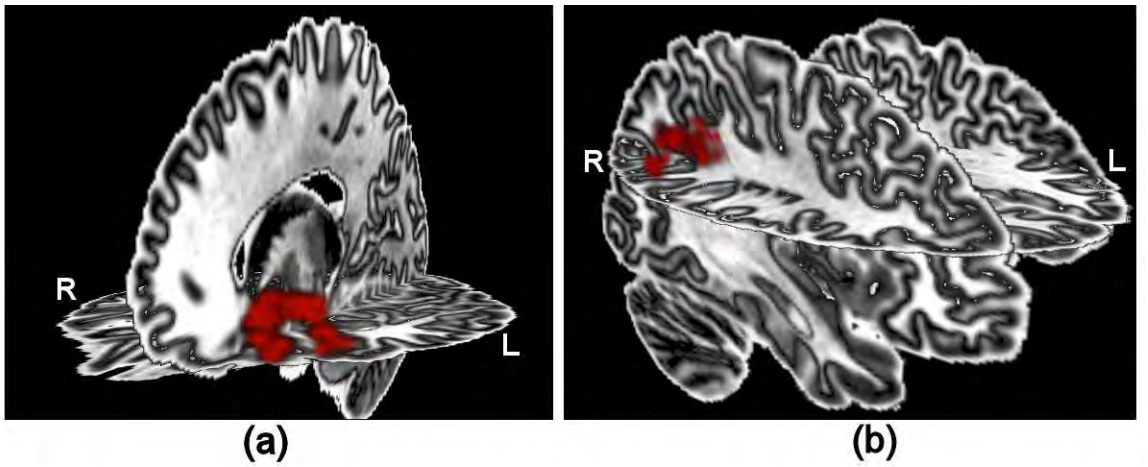

Figure 10: Volumetric views of regions showing less FC in infected children compared to uninfected children with a seed in the a) default mode and b) executive control networks respectively.

4.4.3 ASSOCIATIONS OF CONNECTIVITY AND CLINICAL MEASURES AMONG INFECTED CHILDREN

Clusters with significant associations between the clinical measure CD4/CD8 at enrollment and FC values were found in two RSNs, as summarized in Table 8. Correlations are between CD4/CD8 measures and the average z-score of the cluster.

Table 8: Clusters and networks showing significant correlations between the clinical measure CD4/CD8 at time of enrollment and FC values in the thresholded RSNs of interest. Shown in the columns are: *r*, the average Pearson correlation of the z-score in the cluster with the clinical measure; *p*, the significance value; the number of voxels in the cluster; the coordinates of the peak value in the cluster; and the anatomical location in the Talairach atlas.

Network	*r*	*p-value*	Size (voxels)	Peak coordinate in Talairach space (mm)			Anatomical location
				x	y	z	
Dorsal attention	+0.76	0.0001	31	19.5	64.5	29.5	L precuneus
Auditory	+0.65	0.0004	28	-58.5	37.5	-3.5	R middle temporal gyrus

In the dorsal attention network, we found a significant increase in connectivity in a cluster in the left precuneus with increasing CD4/CD8; and in the auditory network, we found a significant increase in connectivity in a cluster in the right middle temporal gyrus with increasing CD4/CD8. Figure 11 shows the spatial locations of these regions in the brain, both results are positive correlations. Also shown in the figure are the corresponding correlation graphs, in which the average *Z*-score for the region is plotted against the clinical measure for each participant. Treatment arms are shown in different colors.

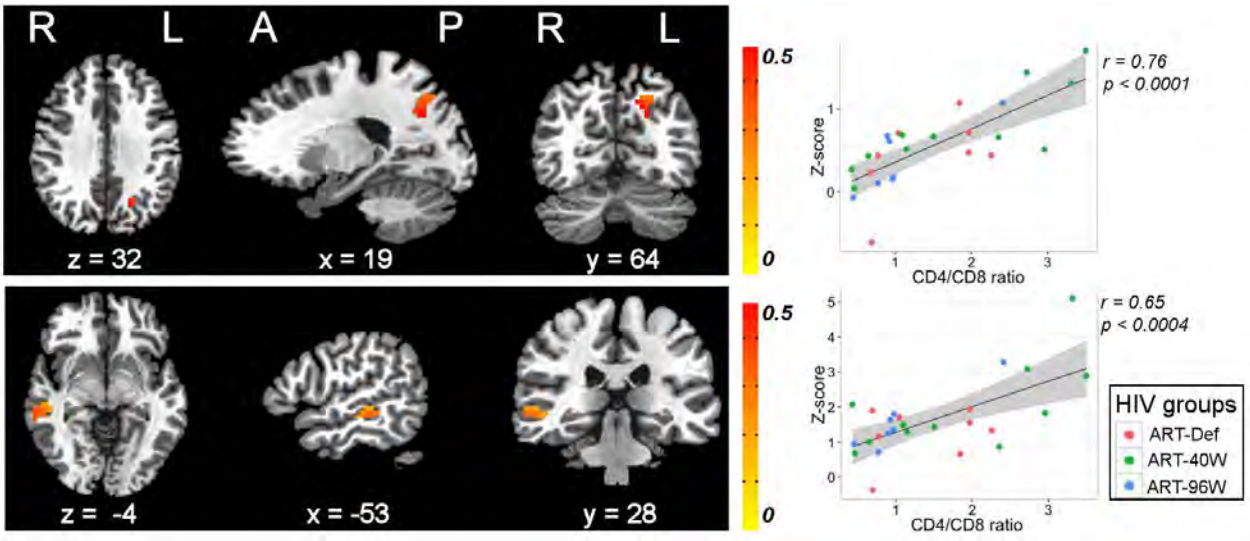

Figure 11: (Left) Brain maps of clusters that exhibited significant associations between CD4/CD8 at enrollment and FC in the dorsal attention (top) and auditory (bottom) networks. (Right) Correlation graphs showing average *Z*-scores over the regions of interest against clinical measures.

4.5.4 WITHIN UNINFECTED, EXPOSED VS. UNEXPOSED, USING ICA AND SCA

No significant clusters showed FC differences between the exposed and unexposed uninfected children in any of the RSNs using ICA. However, using SCA, the voxel-wise two sample t-test examining FC between the seed regions and the whole-brain revealed a number of significant clusters where exposed children showed higher connectivity compared to unexposed children. Fifteen clusters were located across five networks including the default mode, posterior default

mode, executive control, motor and salience networks, as shown below in Table 9 and Figure 12.

There were no overlaps between the clusters of significant difference obtained from this analysis (i.e., exposed vs. unexposed) and the main group level analysis of infected vs. uninfected using SCA. In addition, while the mean Z-scores in the SCA-derived (infected vs. uninfected) clusters were higher in the exposed children compared to the unexposed group, a two sample t-test showed that the differences were not significant.

Table 9: Regions where exposed uninfected children have greater connectivity than that in unexposed children, obtained using SCA. The peak coordinates, size and the anatomical location of each cluster in the Talairach atlas are shown. Labels in the final column refer to the visualizations in Figure 9.

Seed information			**Exposed > unexposed**					
Seed #	**Network**	**Seed location**	**Size (voxels)**	**Peak Coordinate**			**Anatomical location**	**Label**
				x	**y**	**z**		
9	DMN	L medial frontal gyrus	83	-64.5	10.5	17.5	R postcentral gyrus	*a*
			49	49.5	13.5	32.5	L precentral gyrus	*b*
10	DMN	L cingulate gyrus	54	-28.5	25.5	53.5	R precentral gyrus	*c*
4	pDMN	R cingulate gyrus	69	-7.5	7.5	35.5	R cingulate gyrus	*d*
12	Motor	R postcentral gyrus	84	-49.5	-46.5	-3.5	R middle frontal gyrus	*e*
			78	1.5	-37.5	14.5	L anterior cingulate	*f*
			49	40.5	-34.5	14.5	L middle frontal gyrus	*g*
7	Salience	L insula	64	58.5	31.5	29.5	L inferior parietal lobule	*h*
			48	-1.5	7.5	50.5	R medial frontal gyrus	*i*
			45	16.5	70.5	-0.5	L lingual gyrus	*j*
8	Salience	R anterior cingulate	90	-52.5	4.5	5.5	R superior temporal gyrus	*k*
			67	-4.5	73.5	26.5	R precuneus	*l*
			67	46.5	13.5	29.5	L precentral gyrus	*m*
			65	49.5	13.5	11.5	L precentral gyrus	*n*
16	Executive control	R middle frontal gyrus	53	10.5	28.5	-3.5	L thalamus	*o*

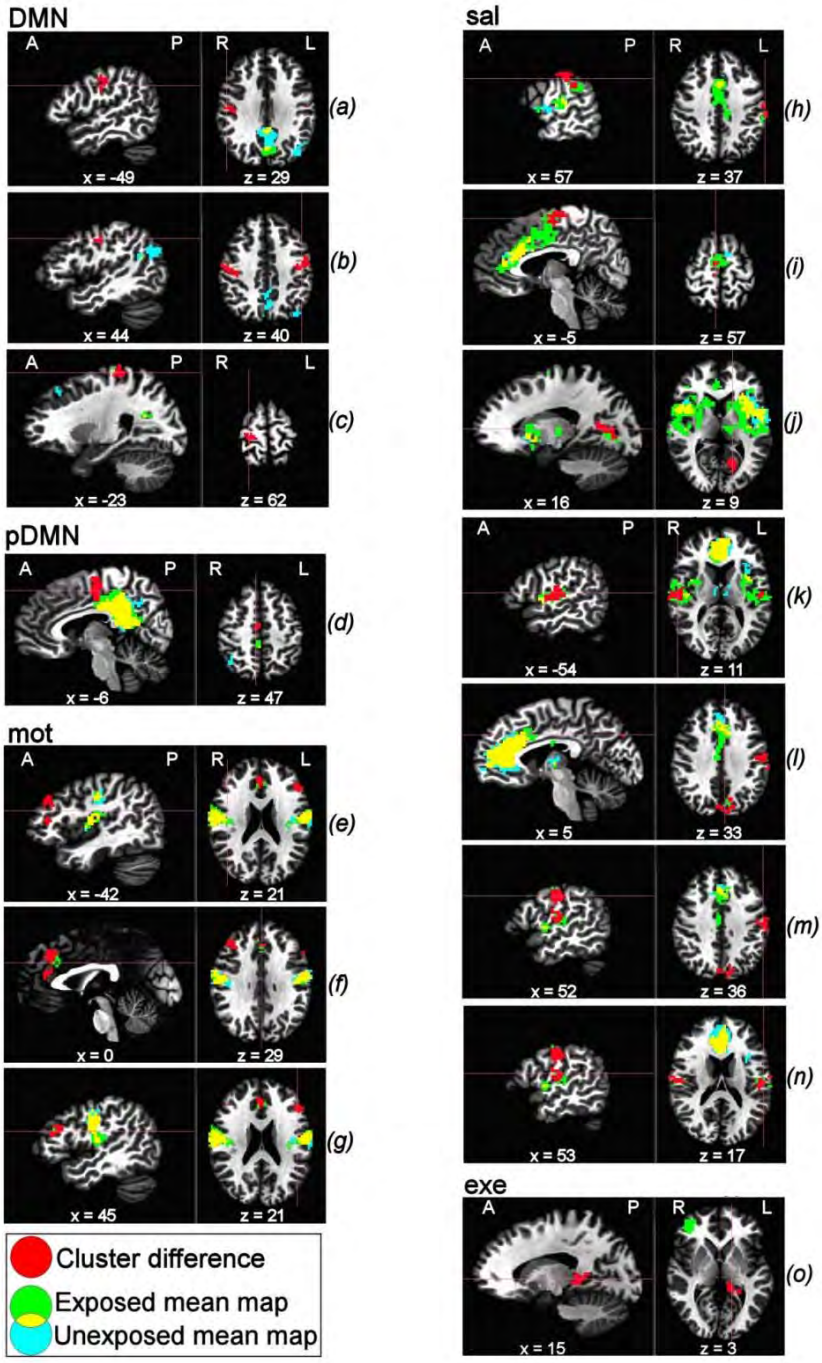

Figure 12: Regions of significantly increased FC within the exposed group compared to unexposed group (shown in red) were observed with seeds in the default mode network (DMN), posterior default mode network (pDMN), motor network (mot), salience network (sal) and executive control network (exe). The mean maps of the exposed children are shown in green and those of the unexposed children in blue, with overlaps in yellow. No clusters of unexposed > exposed were observed. The slice numbers in Talairach space are shown at the base of each panel. The alphabet labels *(a – o)* are used as a reference for the tabulated details shown in Table 9.

5. DISCUSSION

The purpose of this study was to examine the effects of HIV infection and HAART on developing functional brain networks using RS-fMRI. RSFC was compared between HIV infected and uninfected children at age 7, both within the observed RSNs (using ICA) and across the whole brain (using SCA). In addition, we investigated the relationship between clinical measures and resting state parameters to examine the impact of immune system health in infancy on functional brain networks in later development. Lastly, within the HIV uninfected children, we explored the possible effects of HIV exposure on functional networks.

A large motivating factor for conducting this study is the heterogeneous nature of previous pediatric and adult HIV studies, specifically regarding the usage of ART regimens and age range of participants in pediatric HIV studies. The majority of HIV studies have either used ART-naïve HIV infected participants, or have included participants on ART with quite varied initiation times, duration of usage, and particular regimen being used (see, e.g., Hoare et al., 2014; Laughton et al., 2013; Sherr et al., 2009). Table 10 summarizes information regarding the number of participants, age range of participants, tests conducted and treatment being received for a number of previous HIV studies.

The nine networks extracted in this study corresponded visually to standard RSNs; in particular, we compared the maps with two previous pediatric RS-fMRI studies. One study used a group of 65 healthy controls aged 9-15 years (Thomason et al., 2011) and the other comprised of 18 children aged 5-8 years (de Bie et al., 2012). It should be noted that the de Bie et al. (2012) 'control' group consisted of children born small for gestational age (SGA) with postnatal catch-up growth and children born appropriate for gestational age (AGA) and therefore may provide less of a direct comparison for the cohort in the present study. Both Thomason et al. (2011) and our study identified a number of higher cognitive function networks, such as the default mode, executive control and salience networks; however, a dorsal attention network was found in this study, which was not present in theirs. Additional differences included that the DMN was split into two components in this study (in the de Bie et al. (2012) study, the DMN was split into three components) and that Thomason et al. (2011) observed the executive control network split into bilateral (i.e., L and R) components. With regards to the lower-order sensorimotor networks, all of the studies found a visual, motor and auditory network. However, in this study and in de Bie et al. (2012), the visual network was split into the lingual gyrus and occipital lobe components. The comparisons between the RSNs extracted from this study with those from Thomason et al.

Table 10: Summarized information from selected prior HIV studies related to the present work, including: number of participants, age range of participants, tests conducted and treatment regimens received. ANTP, Amsterdam neuropsychological tasks program; BSID, Bayley scales of infant development; KABC, Kauffman assessment battery for children; WISC, Wechsler intelligence scale for children; WAIS, Wechsler adult intelligence scale; WPPSI, Wechsler preschool and primary scales of intelligence; '-R', revised.

Study	Participants (infected, uninfected)	Age range (years)	Test conducted	Treatment received
Bagenda, 2006	28 HIV+, 79 HIV-	6-9	KAB; and others	ART naïve
Boivin et al., 1995	14 HIV+, 36 HIV-	0-2	KAB; and others	ART naïve
Chao et al., 2012	139 HIV+	4-19	Hearing tests	HAART experienced
Chase et al., 2000	114 HIV+, 481 HIV-	0-2.5	BSID	ART naïve (with potential treatment in parallel study, see Sheon et al. (2012))
Gay et al., 1995	28 HIV+, 98 HIV-	0-2	BSID	Receiving AZT
Koekkoek et al., 2006	34 HIV+	4-12	ANTP	16 starting HAART, 7 untreated, 11 HAART stable
Koekkoek et al., 2008	22 HIV+	6-17	ANTP	18 HAART stable, 2 starting HAART, 2 HAART naïve
Lindsey et al., 2007	91 HIV+, 838 HIV-	0.5-3	BSID	HAART-naïve and HAART-experienced
Malee et al., 2009	1429 HIV+	3-18	BSID; WISC-III; WAIS-III	HAART stable
Martin et al., 2006	41HIV+	6-16	WISC-III; CT scans	HAART stable
McGrath	55 HIV+, 221 HIV-	0.5-1.5	BSID	ART-naïve
Melrose et al., 2007	11 HIV+, 11 HIV-	29-52	WAIS-III; and others	10 ART
Morgan et al., 2010	60 HIV+, 35 HIV-	34-52	WAIS-III; and others	45 HAART, 15 HAART naïve
Nachman et al., 2011	319 HIV+	6-17	WAIS-IV; and others	Receiving HAART, HAART stable
Nozyce et al., 2006	274 HIV+	2-17	BID; WISC-III; WPPSI-R	Receiving ART
Qiu et al., 2011	13 HIV+, 13 HIV-	45.5±5.4	**RS-fMRI**	Unspecified
Raskino et al., 1999	831 HIV+	0-18	BSID; WISC-R; WAIS-R; and others	Receiving ART
Ruel et al., 2012	300 HIV+, 601 HIV-	6-12	KAB; and others	ART naïve
Taipale et al., 2011	78HIV+, 78 HIV-	0-15	Hearing tests	36 receiving ART
Thomas et al., 2013	58 HIV+, 53 HIV-	41±14	**RS-fMRI**	Receiving HAART
Van Rie et al., 2008	35 HIV+, 125 HIV-	1.5-6	BSID; and others	ART-naïve, less than 1 week of ART

(2011) and de Bie et al. (2012) indicate that RSNs are present and, in general, can be robustly reproduced in pediatric participants. It should be noted that we utilized 20 components in the ICA; Thomason et al. (2011) used 34 and de Bie et al. (2012) used 28. Additionally, the differences in sample size and exact processing procedures are factors that may contribute to differences across these studies.

Contrary to our preliminary expectations, we did not observe significant group differences in RSFC between infected and uninfected children within any of the nine RSNs using ICA. We then used SCA to explore group differences between specific seed regions within each RSN and their whole brain connectivity. The technique of SCA yielded two significant clusters of reduced FC in the infected children compared to uninfected children. Specifically, reduced connectivity was observed between a seed in the left cingulate gyrus of the DMN and a cluster in the left middle frontal gyrus, as well as between a seed in the right middle frontal gyrus of the executive control network and a cluster in the right supramarginal gyrus. In both cases, the resulting cluster was within the same network as the seed, signifying diminished intranetwork FC within the DMN and executive control networks of HIV infected children.

Contrary to one of our initial hypotheses, we did not observe reduced FC within the motor network of HIV infected children. This may be because motor deficits are often observed and reported in HIV infected infants and children younger than 6 years old (Van Rie et al., 2008; Abubakar et al., 2008; Bagenda et al., 2006; McGrath et al., 2006; Chase et al., 2000; Gay et al., 1995; Boivin et al., 1995); furthermore, in the majority of the studies that previously reported motor deficits, the HIV infected children were ART naïve. Two studies have reported improved motor functioning in HIV infected infants and children under the age of 3 years with the use of treatment (combination therapy and HAART, respectively) (Lindsey et al., 2007; Raskino et al. 1999), suggesting motor deficits may be less severe (or reversed) if treatment is initiated early.

Sensorimotor networks in children between the ages of 5-8 years old have shown functional organization similar to that of a mature adult, while some of the higher order cognitive functional networks (including the DMN and executive control network) are still fragmented at this age (de Bie et al. 2012). As such, a number of RS-fMRI studies have focused specifically on the development of the DMN and executive control networks in healthy children aged between 7-9 years (Superkar et al., 2010; Fair et al., 2008; Fair et al., 2007; Davidson et al., 2006; Anderson 2002;) as these networks are experiencing a more dramatic development during this age range whereby FC changes are occurring.

Specifically, it has been found that at this age, the DMN is only sparsely connected and is still maturing into an interconnected network; compared to the more extensive and more connected DMN observed in adults (Superkar et al., 2010; Fair et al 2008). Therefore, reduced FC within both the default mode and executive control networks may imply either delayed maturation within HIV infected children in these higher cognitive functional networks or network alterations. Since RS-fMRI is related to the extent of myelination connecting the brain regions (Greicius et al., 2009; Hagmann et al., 2008), the findings of this study possibly reflect reduced myelination along the fibers running between the seed and resulting clusters within the default mode and executive control networks of HIV infected children. The DTI data from this cohort is in the process of being analyzed and may generate white matter microstructural deficits to provide supporting evidence of this. In addition, graph theory analysis would provide additional insight into how integrated the networks are within this cohort.

The formation of the DMN into an integrated circuit has been linked to improved memory processing due to the development of higher-order strategic organizations, with the DMN being predominantly responsible for the retrieval of episodic memories (Kim et al., 2011; Andrews-Hanna et al., 2010; Grecius et al., 2008; Frannson et al., 2006; Grecius et al., 2004; Grecius et al., 2003). On the other hand cognitive flexibility, goal setting, and information processing are undergoing a critical stage of development in the executive control network at this age, corresponding to the growth spurt in the frontal lobe (Fair et al., 2007; Anderson, 2002).

In this study, reduced FC in HIV infected children was observed specifically in the frontal gyri of both the executive control and default mode networks. Several previous pediatric HIV studies have shown various aspects of executive functioning to be affected in HIV infected children, including: cognitive functioning, processing speed, verbal fluency, visual spatial memory and cognitive flexibility (Ruel et al., 2012; Nachman et al., 2011; Malee et al., 2009; Koekkoek et al., 2008; Martin et al., 2006; Nozyce et al., 2006; Wachsler-Felder & Golden, 2002). All of these studies used age-appropriate neuropsychological assessments (see Table 10) to assess various aspects of cognitive functioning.

No RS-fMRI studies have been conducted previously on HIV infected children. However, a few RS-fMRI studies have been conducted on HIV infected adults, and some of their findings overlap strikingly with the results of this study. For example, HIV infected adults showed reduced FC within the default mode and executive control networks (Thomas et al., 2013); along with reduced resting state regional homogeneity (ReHo) within a number of regions of the

DMN (Qiu et al., 2011). In these studies, the cingulate gyrus (Qiu et al., 2011) and PCC (Thomas et al., 2013) in the DMN were specifically implicated as loci of FC differences; in the present study we observed a FC difference between the left cingulate gyrus and left middle frontal gyrus of the DMN. Therefore, evidence suggests that regions of both the executive and default mode network are implicated in HIV infected children and adults.

A recent pilot study in Cameroon investigated HIV associated neurocognitive disorders among adult AIDS patients, non-AIDS patients and uninfected controls (Kanmogne et al., 2010). The characteristics of the 'non-AIDS' cohort from the Cameroon study most closely matched those of the 'HIV infected' children in our study, as members of both groups are HIV infected without AIDS. The Kanmogne et al. (2010) study used 19 neuropsychological (NP) measures across the three groups to investigate the effect of HIV on seven domains of cognitive ability. The scores from these NP tests were converted to Z-scores (using the controls' mean and standard deviation) in order to conduct across group comparisons. The resulting neurocognitive findings overlapped considerably with the observed FC network deficits in the present work; see Figure 13 for a summary of the neurocognitive findings from Kanmogne et al. (2010).

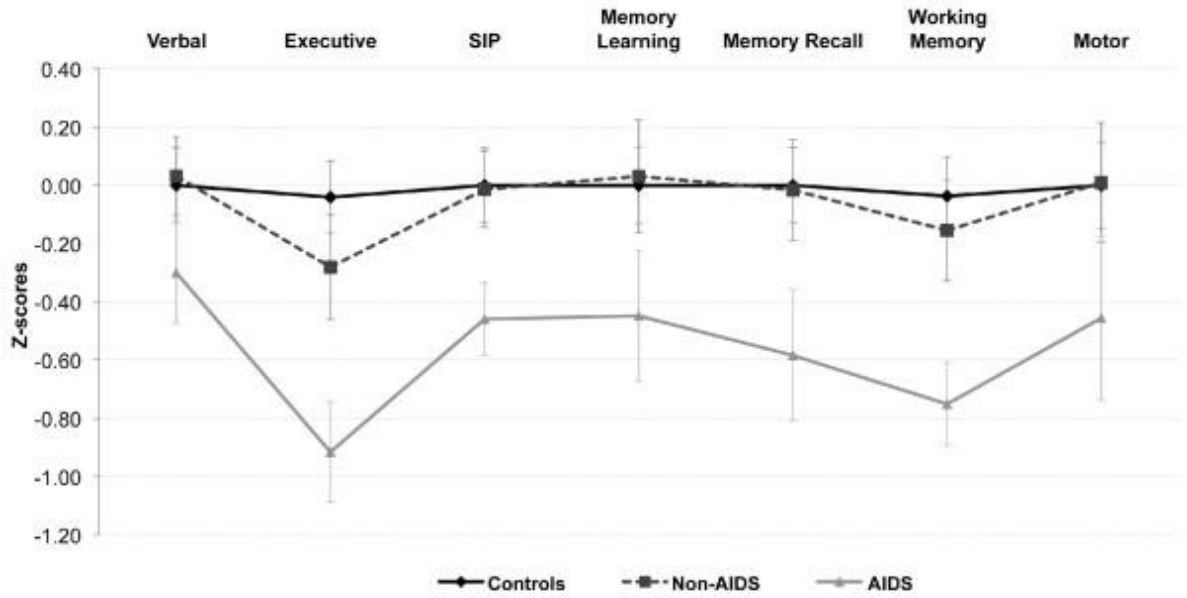

Figure 13: Figure 1 from Kanmogne et al. (2010). The three bars represent AIDS patients, non-AIDS patients (e.g. HIV infected patients) and controls (e.g. HIV uninfected).

Four of the domains showed significant difference between AIDS patients and controls: executive functioning, speed of information processing (SIP), memory recall and working memory. Furthermore, the NP test score results were mirrored by the non-AIDS group, which showed largest impairments for the executive functioning and working memory domains. Both of these capacities rely on the executive control network (Alvarez & Emory, 2006; Blakemore & Choudhury, 2006). Additionally, the PCC in the DMN has been shown to directly support memory retrieval (McCormick et al., 2014; Sestieri et al., 2011; Maddock et al., 2001), and recent studies have also shown strong associations between working memory and the DMN (Piccoli et al., 2015; Pyka et al., 2009).

Previous studies conducted on HIV infected adults have also demonstrated memory retrieval and episodic memory processing to be impaired (Morgan et al., 2010; Melrose et al., 2007). However, we could not find any pediatric HIV studies that showed memory recall impairments in infected children; this may be because the majority of clinical tests performed on pediatric subjects are focused on the aspects of memory processing related to executive functioning (i.e. working memory, prospective memory). Two pediatric HIV studies have shown working memory to be impaired in HIV infected children, with the bulk of these children being stable on HAART (Koekkoek et al., 2008; Martin et al., 2006).

To examine the impact of immune system health during infancy on the development of network connectivity, we investigated the association between the quantitative clinical measure, CD4/CD8, at enrollment and FC within the RSNs of HIV infected children. CD4/CD8 at enrollment provides a measure of immune system health of the child in infancy before the initiation of treatment. We observed two significant positive associations between CD4/CD8 and FC within the dorsal attention and auditory networks. Children with weaker immune systems in infancy (i.e., with lower CD4/CD8, characterized by decreased CD4 helper cells and increased CD8 suppressor/killer cells) had lower FC within a region of the left precuneus from the dorsal attention network. The main function of the dorsal attention network is to identify relevant incoming sensory content related to the current task (Ptak, 2012; Ozaki, 2011; Corbetta & Shulman, 2002). This result suggests that children with higher CD4/CD8 in infancy may at age 7 years deal better with incoming sensory content.

Within the auditory network, increased CD4/CD8 at enrollment was associated with increased connectivity in a cluster in the right middle temporal gyrus. In processing auditory information, this network plays a significant role in hearing and speech (Hackett, 2011; Zatorre et al., 2002).

Previous research has indicated hearing to be impaired in cohorts of HIV infected children from Peru and Angola (Chao et al., 2012; Taipale et al., 2011). In the present study, the significant correlation between the cluster in the auditory network and CD4/CD8 indicates that higher baseline immune system health at time of enrollment is associated with higher connectivity within the auditory network.

Within the plotted graphs of CD4/CD8 correlations with FC, there was no effect of treatment arm. This suggests that the observed connectivity at age 7 years depended much more strongly on the children's early immune health (time of enrollment 6 – 8 weeks of age) than on the ART start time (varying from 7 to 76 weeks). This result indicates that earlier treatment is warranted, in order to maintain the highest levels of immune health during infancy, and thereby reduce long lasting effects of HIV infection during development.

Lastly, an exploratory analysis was conducted between the unexposed and exposed uninfected children in order to investigate the possible impacts of HIV exposure itself. The sample size for this analysis was small (8 exposed and 10 unexposed), which limited the statistical power of the results. No group level differences were found between any of the RSNs of unexposed and exposed children using ICA. However, SCA revealed sixteen clusters where connectivity differed between unexposed and exposed children, from seeds within the DMN, pDMN, salience, executive control and motor networks. For each of these differences, exposed children exhibited a higher FC compared to unexposed children, which was contrary to what was expected. Also, exposed children had a higher Z-score compared to unexposed children in the clusters from the default mode and executive control networks that were extracted from the SCA of infected and uninfected children, but the difference was not significant. Therefore, it does not seem that it was solely the HIV exposed children driving the group level differences observed between the infected and uninfected groups. Much larger exposed and unexposed group sizes would be required for an in-depth analysis of exposure-related effects.

ICA and SCA focus on different connectivity measures, specifically, ICA produces RSN's and SCA examines full brain connectivity to one specific region. When examining differences between groups using RSFC networks from ICA, we found no differences. However, we found differences using SCA and this may be attributed to the fact that SCA is not limited to the network boundaries or the specific time-series of an independent component in ICA.

The study contributed to our current understanding of HIV infected children stable on HAART by showing that their RSN's are robust, which is significant as it indicates that overall, the

functional brain networks of these children are intact. In addition, FC deficits with SCA in HIV infected children demonstrate alterations in connectivity that may be due to developmental delays, while regions showing FC deficits associated with CD4/CD8 at enrollment may be part of networks that develop early and as such are particularly vulnerable to immune health in the first 6 weeks of life.

One overall limitation of this study was the relatively small sample size, making investigation of differences between treatment arms within the infected group, as well as differences between exposed and unexposed children within the uninfected group, difficult. The small sample sizes of the subgroups do not allow for meaningful interpretation of statistical differences. External factors such as prenatal drug exposure, poverty, malnutrition, social stigmatization and the home environment, as well as treatment interruption, were not explicitly controlled for in this study; however, 'current treatment' was consistent across all treatment arms, as all infected children were receiving HAART at time of scanning. In addition, even though we controlled for possible differences due to sex, only the subgroup of uninfected exposed children were equally matched for females and males. The majority of other subgroups had more females, and therefore a larger cohort of HIV infected males may be required.

The present work examined functional networks at one time point and modality (i.e. RS-fMRI at age 7 years old) within a larger multimodal, longitudinal study. Analysis of the data at subsequent ages will allow for more in depth analysis of functional changes in development over time, along with a more detailed longitudinal description of the impact of HIV and HAART on the developing brain. Future work should incorporate the findings of this study with other modalities that were acquired at age 7 years old, which included structural MRI, DTI, and MRS. This will enable overarching patterns of effects to be investigated and related to the functional deficits found in this study. In addition, neuropsychological and behavioral data acquired at age 7 could also be correlated to the findings of this study.

6. CONCLUSION

In summary, we found reduced FC within both the default mode and the executive control networks of HIV infected children compared to uninfected controls. Previous RS-fMRI studies in HIV infected adults have observed similar FC reductions in these networks, suggesting that they are particularly sensitive to the effects of HIV infection. Furthermore, deficits in neurocognitive abilities associated with both networks have been reported in HIV infected adults and children. In children, these networks are still undergoing critical development at this age so that FC reductions may point to delayed network maturation that could have long-term implications for cognitive functioning, information processing and memory recall ability. Direct comparisons of FC results with neurocognitive assessments are necessary in order to further explore the relationship between outcomes and FC reductions.

In addition, we examined the associations of RSN properties with clinical measures, observing positive associations between the CD4/CD8 at the time of enrollment with FC within regions of the dorsal attention and auditory networks. These associations were independent of treatment arm, and suggest that lower connectivity at age 7 years in these networks is a result of poor immune system health in early infancy at approximately 6 – 8 weeks of age. These results support the current trend towards immediate ART initiation at birth in order to reduce long-term effects of the virus on healthy brain development; early treatment (7-12 weeks of age) was not observed to be associated with functional network changes in this study.

REFERENCES

Abou-Elseoud, A., Starck, T., Remes, J., Nikkinen, J., Tervonen, O., & Kiviniemi, V. (2010). The effect of model order selection in group PICA. *Human Brain Mapping, 31,* 1207–1216.

Abubakar, A., Van Baar, A., Van De Vijver, F. J. R., Holding, P., & Newton, C. R. J. C. (2008). Paediatric HIV and neurodevelopment in sub-Saharan Africa: A systematic review. *Tropical Medicine and International Health, 13(7),* 880–887.

Alvarez, J. A., & Emory, E. (2006). Executive function and the frontal lobes: A meta-analytic review. *Neuropsychology Review, 16(1),* 17–42.

Anderson, P. (2002). Assessment and Development of Executive Function (EF) During childhood. *Child Neuropsychology, 8(2),* 71–82.

Andrews-Hanna, J. R., Reidler, J. S., Huang, C., & Buckner, R. L. (2010). Evidence for the default network's role in spontaneous cognition. *Journal of Neurophysiology, 104(1),* 322–35.

Badri, M., Cleary, S., Maartens, G., Pitt, J., Bekker, L.-G., Orrell, C., & Wood, R. (2006). When to initiate highly active antiretroviral therapy in sub-Saharan Africa? A South African cost-effectiveness study. *Antiviral Therapy, 11(1),* 63–72.

Bagenda, D., Nassali, A., Kalyesubula, I., Sherman, B., Drotar, D., Boivin, M. J., & Olness, K. (2006). Health, neurologic, and cognitive status of HIV-infected, long-surviving, and antiretroviral-naive Ugandan children. *Pediatrics, 117(3),* 729–740.

Beckmann, C. F., DeLuca, M., Devlin, J. T., & Smith, S. M. (2005). Investigations into resting-state connectivity using independent component analysis. *Philosophical Transactions of the Royal Society of London, 360,* 1001–13.

Belcher, A. M., Yen, C. C., Stepp, H., Gu, H., Lu, H., Yang, Y., Silva, A. C., & Stein, E. A. (2013). Large-scale brain networks in the awake, truly resting marmoset monkey. *The Journal of Neuroscience, 33(42),* 16796–804.

Birn, R. M., Diamond, J. B., Smith, M. A, & Bandettini, P. A. (2006). Separating respiratory-variation-related fluctuations from neuronal-activity-related fluctuations in fMRI. *NeuroImage, 31(4),* 1536–48.

Biswal, B., Yetkin, F. Z., Haughton, V.M., & Hyde, J.S. (1995): Functional connectivity in the motor cortex of resting human brain using echo-planar MRI. *Magnetic resonance in medicine, 34(9)*, 537-541.

Biswal, B., Mennes, M., Zuo, X.-N., Gohel, S., Kelly, C., Smith, S.M., Beckmann, C.F., Adelstein, J.S., Buckner, R.L., Colcombe, S., Dogonowski, A.-M., Ernst, M., Fair, D., Hampson, M., Hoptman, M.J., Hyde, J.S., Kiviniemi, V.J., Kotter, R., Li, S.-J., Lin, C.-P., Lowe, M.J., Mackay, C., Madden, D.J., Madsen, K.H., Margulies, D.S., Mayberg, H.S., McMahon, K., Monk, C.S., Mostofsky, S.H., Nagel, B.J., Pekar, J.J., Peltier, S.J., Petersen, S.E., Reidl, V., Rombouts, S.A.R.B., Rypma, B., Schlaggar, B.L., Schmidt, S., Seidler, R.D., Siegle, G.J., Sorg, C., Teng, G.-J., Veijola, J., Villringer, A., Walter, M., Wang, L., Weng, X.-C., Whitfield-Gabrieli, S., Williamson, P., Windischberger, C., Zang, Y.-F., Zhang, H.-Y., Castellanos, F.X. & Milham, M.P. (2010). Toward discovery science of human brain function. *Proceedings of the National Academy of Sciences, 107,* 4734–4739.

Blakemore, S.-J., & Choudhury, S. (2006). Development of the adolescent brain: implications for executive function and social cognition. *Journal of Child Psychology and Psychiatry, and Allied Disciplines, 47,* 296–312.

Bofill, M., Janossy, G., Lee, C. A, MacDonald-Burns, D., Phillips, A. N., Sabin, C., Timms, A., Johnson, M. A., & Kernoff, P. B. (1992). Laboratory control values for CD4 and CD8 T lymphocytes. Implications for HIV-1 diagnosis. *Clinical and Experimental Immunology, 88,* 243–252.

Boivin, M. J., Green, S. D. R., Davies, A. G., Giordani, B., Mokili, J. K. L., & Cutting, W. A. M. (1995). A preliminary Evaluation of the Cognitive and Motor effects of Pediatric HIV infection in Zairian children. *Health Psychology, 14,* 13-21

Branson, B. M., Owen, S. M., Wesolowski, L. G., Bennett, B., Werner, B. G., Wroblewski, K. E., & Pentella, M. A. (2014). Laboratory Testing for the Diagnosis of HIV Infection Updated Recommendations. *Centers for Disease Control and Prevention and Association of Public Health Laboratories.*

Broãœwers, P. I. M., Decarli, C., Heyes, M. P., Moss, H. A., Wolters, P. L., Tudor-williams, G., Civitello, L. A., & Pizzo, P. A. (1996). Neurobehavioral Manifestations of Symptomatic

HIV-1 Disease in Children : Can Nutritional Factors Play a Role?. *American Institute of Nutrition, 126,* 2651S-2662S.

Bruck, I., Tahan, T. T., Cruz, C. R., Martins, L. T., Antoniuk, S. a, Rodrigues, M., de Souza, S. M., & Bruyn, L. R. (2001). Developmental milestones of vertically HIV infected and seroreverters children: follow up of 83 children. *Arquivos de Neuro-Psiquiatria, 59(3-B),* 691–5.

Buttner, A. & Weis, S. (2005). HIV-1 Infection of the Central Nervous. *Forensic Pathology Reviews, 3.*

Calhoun, V. D., Adali, T., Pearlson, G. D., & Pekar, J. J. (2001). A Method for Making Group Inferences from Functional MRI Data Using Independent Component Analysis. *Human Brain Mapping, 14,* 140–151.

Chakraborty, R. (2008). Update on HIV-1 infection in children. *Paediatrics and Child Health, 18(11),* 496–501.

Chase, C., Ware, J., Hittelman, J., Blasini, I., Smith, R., Llorente, A., Anisfeld E., Diaz, C., Fowler, M. G., Moye, J., & Kaligh, L., I. (2000). Early Cognitive and Motor Development Among Infants Born to Women Infected with Human Immunodeficiency Virus. *Pediatrics, 106(2),* 1-10.

Chao, C.K., Czechowicz, J. A., Messner, A. H., Alarcon, J., Kolevic Roca, L., Larragan Rodriguez, M.M., Gutierrez Villafuerte, C., Montano, S.M., & Zunt, J.R. (2012). High Prevalence of Hearing Impairment in HIV-Infected Peruvian Children. *Otolaryngology -- Head and Neck Surgery, 146(2),* 259–265.

Chirboga, C., Fleshman, S., Champion, S., Gaye-Robinson, L., & Abrams, E. J. (2005). Incidence and prevalence of HIV encephalopathy in children with HIV infection receiving HAART. *Journal of Pediatrics, 146,* 402–7.

Chouquet, C., Richardson, S., Burgard, M., Blanche, S., Mayaux, M. J., Rouzioux, C., & Costagliola, D. (1999). Timing of human immunodeficiency virus type 1 (HIV-1) transmission from mother to child: bayesian estimation using a mixture. *Statistics in Medicine, 18(7),* 815–33.

Cole, D. M., Smith, S. M., & Beckmann, C. F. (2010). Advances and pitfalls in the analysis and interpretation of resting-state FMRI data. *Frontiers in Systems Neuroscience, 4(8),* 1–15.

Coplan, J., Contello, K.A., Cunningham, C.K., Weiner, L.B., Dye, T.D., Roberge, L., Wojtowycz, M.A., & Kirkwood, K. (1998). Early Language Development in Children Exposed to or Infected With. *Pediatrics, 102(1),* 1–4.

Corbetta, M., & Shulman, G. L. (2002). Control of goal-directed and stimulus-driven attention in the brain. *Nature Reviews Neuroscience, 3,* 201–215.

Coscia, J. M., Christensen, B. K., Henry, R. R., Wallston, K., Radcliffe, J., & Rutstein, R. (2001). Effects of home environment, socioeconomic status, and health status on cognitive functioning in children with HIV-1 infection. *Journal of Pediatric Psychology, 26(6),* 321–9.

Cotton, M.F., Violari, A., Otwombe, K., Panchia, R., Dobbels, E., Rabie, H., Josipovic, D., Liberty, A., Lazarus, E., Innes, S., Van Rensburg, A.J., Pelser, W., Truter, H., Madhi, S. A., Handelsman, E., Jean-Philippe, P., McIntyre, J. A., Gibb, D.M., & Babiker, A.G. (2013). Early time-limited antiretroviral therapy versus deferred therapy in South African infants infected with HIV: Results from the children with HIV early antiretroviral (CHER) randomised trial. *The Lancet, 382*, 1555–1563.

Cox, R.W. (1996). AFNI: software for analysis and visualization of functional magnetic resonance neuroimages. *Computers and biomedical research, an international journal, 29(3),* 162–73.

Davidson, M. C., Amso, D., Anderson, L. C., & Diamond, A. (2006). Development of cognitive control and executive functions from 4 to 13 years: Evidence from manipulations of memory, inhibition, and task switching. *Neuropsychologia, 44,* 2037–2078.

De Bie, H.M. A., Boersma, M., Adriaanse, S., Veltman, D.J., Wink, A.M., Roosendaal, S.D., Barkhof, F., Stam, C.J., Oostrom, K.J., Delemarre-van de Waal, H. A., & Sanz-Arigita, E.J. (2012). Resting-state networks in awake five- to eight-year old children. *Human Brain Mapping, 33,* 1189–1201.

De Luca, M., Beckmann, C. F., De Stefano, N., Matthews, P. M., & Smith, S. M. (2006). fMRI resting state networks define distinct modes of long-distance interactions in the human brain. *NeuroImage, 29(4),* 1359–67.

Diamond, G. W., Kaufman, J., Belman, A., Cohen, L. and H., & Rubinstein, A. (1987). Characterization of Cognitive Functioning HIV Infection in a Subgroup of Children with Congenital HIV infection. *Archives of Clinical Neuropsychology, 2,* 245–256.

Diniz, L. M. O., Maia, M. M. M., Camargos, L. S., Amaral, L. C., Goulart, E. M. A., & Pinto, J. A. (2011). Evaluation of long-term immunological and virological response to highly active antiretroviral therapy in a cohort of HIV infected children. *HIV & AIDS Review, 10(3),* 70–75.

Dosenbach, N. U. F., Fair, D. a., Cohen, A. L., Schlaggar, B. L., & Petersen, S. E. (2008). A dual-networks architecture of top-down control. *Trends in Cognitive Sciences, 12(3),* 99–105.

Eisenhut, M. (2012). An update on HIV in children. *Paediatrics and Child Health, 23(3),* 109–114.

Ernst, T., Chang, L., & Arnold, S. (2003). Increased glial metabolites predict increased working memory network activation in HIV brain injury. *NeuroImage, 19(4),* 1686–1693.

Fair, D. A, Dosenbach, N.U.F., Church, J. A, Cohen, A.L., Brahmbhatt, S., Miezin, F.M., Barch, D.M., Raichle, M.E., Petersen, S.E., & Schlaggar, B.L. (2007). Development of distinct control networks through segregation and integration. *Proceedings of the National Academy of Sciences, 104(33),* 13507–12.

Fair, D. A., Cohen, A. L., Dosenbach, N. U., & Church, J. A. (2008). The maturing architecture of the brain's default network. *Proceedings of the National Academy of Science, 105(10),* 4028–4032.

Fahey, J. L., Taylor, J. M., Detels, R., Hofmann, B., Melmed, R., Nishanian, P., & Giorgi, J. V. (1990). The prognostic value of cellular and serologic markers in infection with human immunodeficiency virus type 1. *The New England Journal of Medicine, 322(3),* 166–172.

Fishkin, P. E., Armstrong, F. D., Routh, D. K., Harris, L., Thompson, W., Miloslavich, K., Levy, J. D., Johnson, A., Morrow, C., Bandstra, E. S., Mason, C. A., & Scott, G. (2000). Brief report: relationship between HIV infection and WPPSI-R performance in preschool-age children. *Journal of Pediatric Psychology, 25(5),* 347–51.

Fox, M. D., Snyder, A. Z., Vincent, J. L., Corbetta, M., Van Essen, D. C., & Raichle, M. E. (2005). The human brain is intrinsically organized into dynamic, anticorrelated functional networks. *Proceedings of the National Academy of Science, 102,* 9673–9678.

Fox, M. D., Corbetta, M., Snyder, A. Z., Vincent, J. L., & Raichle, M. E. (2006). Spontaneous neuronal activity distinguishes human dorsal and ventral attention systems. *Proceedings of the National Academy of Sciences, 103,* 10046–10051. doi:10.1073/pnas.0604187103

Fransson, P. (2005). Spontaneous low-frequency BOLD signal fluctuations: an fMRI investigation of the resting-state default mode of brain function hypothesis*. Human Brain Mapping, 26(1),* 15–29.

Fransson, P. (2006). How default is the default mode of brain function? Further evidence from intrinsic BOLD signal fluctuations. *Neuropsychologia, 44(14),* 2836–45.

Gao, W., & Lin, W. (2012). Frontal parietal control network regulates the anti-correlated default and dorsal attention networks. *Human Brain Mapping, 33,* 192–202.

Gay, C. L., Armstrong, F. D., Cohen, D., Lai, S., Hardy, M. D., Swales, T. P., Morrow, C. J., & Scott, B. (1995). The Effects of HIV on Cognitive and Motor Development in Children Born to HIV-Seropositive Women With No Reported Drug Use : Birth to 24 Months. *American Academy of Pediatrics, 96(6),* 1078–1082.

Greicius, M. D., Krasnow, B., Reiss, A. L., & Menon, V. (2003). Functional connectivity in the resting brain: a network analysis of the default mode hypothesis. *Proceedings of the National Academy of Sciences,100(1),* 253–8.

Greicius, M. D., & Menon, V. (2004). Default-mode activity during a passive sensory task: uncoupled from deactivation but impacting activation. *Journal of Cognitive Neuroscience, 16(9),* 1484–92.

Greicius, M. (2008). Resting-state functional connectivity in neuropsychiatric disorders. *Current Opinion in Neurology, 21(4),* 424–30.

Greicius MD, Supekar K, Menon V, Dougherty RF (2009): Resting-state functional connectivity reflects structural connectivity in the default mode network. Cerebral Cortex 19,72–78.

Hackett, T. A. (2011). Information flow in the auditory cortical network. *Hearing Research, 271(1-2),* 133–146.

Hagmann P, Cammoun L, Gigandet X, Meuli R, Honey CJ, Wedeen VJ, Sporns O (2008): Mapping the structural core of human cerebral cortex. PLoS Biol 6,159.

Hair, J. F. Jr., Anderson, R. E., Tatham, R. L. & Black, W. C. (1995). *Multivariate Data Analysis (3rd ed).* New York: Macmillan.

Ham, T., Leff, A., de Boissezon, X., Joffe, A., & Sharp, D. J. (2013). Cognitive control and the salience network: an investigation of error processing and effective connectivity. *The Journal of Neuroscience, 33(16),* 7091–8.

Heine, L., Soddu, A., Comez, F., Vanhaudenhuyse, A., Tshibanda, L., Thonnard, M., Charland-Verville, V., Kirsch, M., Laureys, S., & Demertzi, A. (2012). Resting state networks and consciousness*. Frontiers in Psychology, 3(295),* 1–12.

Hoare, J., Fouche, J.P., Spottiswoode, B., Donald, K., Philipps, N., Bezuidenhout, H., Mulligan, C., Webster, V., Oduro, C., Schrieff, L., Paul, R., Zar, H., Thomas, K., & Stein, D. (2012). A diffusion tensor imaging and neurocognitive study of HIV-positive children who are HAART-naïve “slow progressors.” *Journal of NeuroVirology, 18,* 205–212.

Hoare, J., Ransford, G. L., Phillips, N., Amos, T., Donald, K., & Stein, D. J. (2014). Systematic review of neuroimaging studies in vertically transmitted HIV positive children and adolescents. *Metabolic Brain Disease, 29,* 221–229.

Holroyd, C. B., Nieuwenhuis, S., Yeung, N., Nystrom, L., Mars, R. B., Coles, M. G. H., & Cohen, J. D. (2004). Dorsal anterior cingulate cortex shows fMRI response to internal and external error signals. *Nature Neuroscience, 7(5),* 497–498.

Husain, F. T., & Schmidt, S. A. (2014). Using resting state functional connectivity to unravel networks of tinnitus. *Hearing Research, 307,* 153–162.

Jenkinson, M., Bechmann, C.F., Behrens, T.E., Woolrich, M.W., & Smith, S.M., (2012).FSL. *NeuroImage, 62,* 782-90.

Jezzard, P., Matthews, P., & Smith, S. (2001). *fMRI an introduction to methods*. Oxyford University Press, 1st edition.

Johnson, S. C., Baxter, L. C., Wilder, L. S., Pipe, J. G., Heiserman, J. E., & Prigatano, G. P. (2002). Neural correlates of self-reflection. *Brain, 125*, 1808–1814.

Kanmogne, G.D., Kuate, C.T., Cysique, L. a, Fonsah, J.Y., Eta, S., Doh, R., Njamnshi, D.M., Nchindap, E., Franklin, D.R., Ellis, R.J., McCutchan, J. a, Binam, F., Mbanya, D., Heaton, R.K., & Njamnshi, A.K. (2010). HIV-associated neurocognitive disorders in sub-Saharan Africa: a pilot study in Cameroon. *BMC Neurology, 10*, 1–11.

Kelly, A. M. C., Uddin, L. Q., Biswal, B. B., Castellanos, F. X., & Milham, M. P. (2008). Competition between functional brain networks mediates behavioral variability. *NeuroImage, 39(1),* 527–37.

Kids ART Link Collaboration. (2008). Low risk of death, but substantial program attrition, in pediatric HIV treatment cohorts in Sub-Saharan Africa. *Journal of Acquired Immune Deficiency Syndromes, 49(5),* 523–31.

Kim, H., Daselaar, S. M., & Cabeza, R. (2011). Overlapping brain activity between episodic memory encoding and retrieval: roles of the task-positive and task-negative networks. *NeuroImage, 49(1),* 1045–1054.

Kline, M.W., Fletcher, C. V, Harris, a T., Evans, K.D., Brundage, R.C., Remmel, R.P., Calles, N.R., Kirkpatrick, S.B., & Simon, C. (1998). A pilot study of combination therapy with indinavir, stavudine (d4T), and didanosine (ddI) in children infected with the human immunodeficiency virus. *The Journal of Pediatrics, 132(3 Pt 1),* 543–6.

Koekkoek, S., Eggermont, L., De Sonneville, L., Jupimai, T., Wicharuk, S., Apateerapong, W., Chuenyam, T., Lange, J., Wit, F., Pancharoen, C., Phanuphak, P., & Ananworanich, J. (2006). Effects of highly active antiretroviral therapy (HAART) on psychomotor performance in children with HIV disease. *Journal of Neurology, 253,* 1615–1624.

Koekkoek, S., de Sonneville, L. M. J., Wolfs, T. F. W., Licht, R., & Geelen, S. P. M. (2008). Neurocognitive function profile in HIV-infected school-age children. *European Journal of Paediatric Neurology, 12(4),* 290–7.

Kowala-Piaskowska, A., Mania, A., Barałkiewicz, G., Żeromski, J., & Mozer-Lisewska, I. (2010). Woman living with HIV/AIDS and her child – epidemiological data. *HIV & AIDS Review, 9(3),* 72–78.

Laughton, B., Cornell, M., Boivin, M., & Van Rie, A. (2013). Review article Neurodevelopment in perinatally HIV-infected children : a concern for adolescence. *Journal of the International AIDS Society, 16(1),* 18603.

Lee, M., Smyser, C., & Shimony, J. (2013): Resting-state fMRI: a review of methods and clinical applications. *American Journal of Neuroradiology, 34,* 1866-1872.

Letendre, S., Marquie-Beck, J., Capparelli, E., Best, B., Clifford, D., Collier, A.C., Gelman, B.B., McArthur, J.C., McCutchan, J.A., Morgello, S., Simpson, D., Grant, I., & Ellis, R.J. (2008). Validation of the CNS Penetration-Effectiveness rank for quantifying antiretroviral penetration into the central nervous system. *Archives of Neurology, 65(1),* 65–70.

Lindsey, J. C., Malee, K. M., Brouwers, P., & Hughes, M. D. (2007). Neurodevelopmental functioning in HIV-infected infants and young children before and after the introduction of protease inhibitor-based highly active antiretroviral therapy. *Pediatrics, 119(3),* e681–93.

Linguissi, L.S.G., Bisseye, C., Sagna, T., Nagalo, B.M., Ouermi, D., Djigma, F.W., Pignatelli, S., Sia, J.D., Pietra, V., Moret, R., Nikiema, J.B., & Simpore, J. (2012). Efficiency of HAART in the prevention of mother to children HIV-1 transmission at Saint Camille medical centre in Burkina Faso, West Africa. *Asian Pacific Journal of Tropical Medicine, 5(12),* 991–4.

Liu, F., Guo, W., Liu, L., Long, Z., Ma, C., Xue, Z., Wang, Y., Li, J., Hu, M., Zhang, J., Du, H., Zeng, L., Liu, Z., Wooderson, S.C., Tan, C., Zhao, J., Chen, H. (2013). Abnormal amplitude low-frequency oscillations in medication-naive, first-episode patients with major depressive disorder: a resting-state fMRI study. *Journal of Affective Disorders, 146(3),* 401–6.

Long, X.-Y., Zuo, X.-N., Kiviniemi, V., Yang, Y., Zou, Q.-H., Zhu, C.-Z., Jiang, T.-Z., Yang, H., Gong, Q.-Y., Wang, L., Li, K.-C., Xie, S., & Zang, Y.-F. (2008). Default mode network as revealed with multiple methods for resting-state functional MRI analysis. *Journal of Neuroscience Methods, 171(2),* 349–55.

Lyall, E. G. H. (2002). Paediatric HIV in 2002-a treatable and preventable infection. *Journal of Clinical Virology, 25(2),* 107–19.

Maddock, R. J., Garrett, A. S., & Buonocore, M. H. (2001). Remembering familiar people: the posterior cingulate cortex and autobiographical memory retrieval. *Neuroscience, 104(3),* 667–676.

Madhi, S. A., Adrian, P., Cotton, M. F., McIntyre, J. A., Jean-Philippe, P., Meadows, S., Nachman, S., Kayhty, H., Klugman, K. P., Violari, A. (2010). Effect of HIV Infection Status and Anti-Retroviral Treatment on Quantitative and Qualitative Antibody Responses to Pneumococcal Conjugate Vaccine in Infants. *Journal of infectious diseases, 202, 355–361.*

Malee, K., Williams, P.L., Montepiedra, G., Nichols, S., Sirois, P. A., Storm, D., Farley, J., & Kammerer, B. (2009). The Role of Cognitive Functioning in Medication Adherence of Children and Adolescents with HIV Infection. *Journal of pediatric psychology, 34(2),* 164–175.

Martin, S. C., Wolters, P. L., Toledo-Tamula, M. A., Zeichner, S. L., Hazra, R., & Civitello, L. (2006). Cognitive functioning in school-aged children with vertically acquired HIV infection being treated with highly active antiretroviral therapy (HAART). *Developmental Neuropsychology, 30(2),* 633–657.

Mbugua, K., Holmes, M. J., Hess, A.T., Little F., Cotton M.F., Dobbels E., van der Kouwe A.J.W., Laughton B., Meintjes E.M. (2014). Effects of ART timing and HIV progression on neuro-metabolite levels in basal ganglia at age 5 years. 20th Annual Meeting of the OHBM, Germany. Poster No. 2220

McCormick, C., Protzner, A. B., Barnett, A. J., Cohn, M., Valiante, T. A., & McAndrews, M. P. (2014). Linking DMN connectivity to episodic memory capacity: What can we learn from patients with medial temporal lobe damage? NeuroImage: Clinical, 5, 188–196.

McGrath N., Fawzi W.W., Bellinger D., Robins, J., Msamanga G.I., Manji, K., & Tronick, E. (2006) The timing of mother-to-child transmission of human immunodeficiency virus infection and the neurodevelopment of children in Tanzania. *Pediatric Infectious Disease Journal, 25(1),* 47–52

McKeown, M. J., & Sejnowski, T. J. (1998). Independent component analysis of fMRI data: examining the assumptions. *Human Brain Mapping, 6(5-6),* 368–72.

Melrose, R. J., Tinaz, S., Castelo, J. M. B., Courtney, M. G., & Stern, C. E. (2008). Compromised fronto-striatal functioning in HIV: an fMRI investigation of semantic event sequencing. *Behavioural Brain Research, 188(2),* 337–47.

Miotti, P.G., Taha, T., Kumwenda, N.I., Broadhead, R., Mtimavalye, L., Hoeven, L. Van der, Chiphangwi, J.D., Liomba, G., & Biggar, R.J. (1999). HIV Transmission Through Breastfeeding. *American Medical Asssociation, 282(8),* 744–749.

Miziara, I. D., Filho, B. C. A., & Weber, R. (2006). Oral lesions in Brazilian HIV-infected children undergoing HAART. *International Journal of Pediatric Otorhinolaryngology, 70(6),* 1089–96.

Morgan, E.E., Woods, S.P., Weber, E., Dawson, M.S., Catherine, L., Moran, L.M., & Grant, I. (2010). HIV-associated Episodic Memory impairment: evidence of a possible differntial deficit in source memory for complex visual stimuli. J*ournal of Neuropsychiatry and Clinical Neuroscience, 21(2),* 189–198.

Mowinckel, A. M., Espeseth, T., & Westlye, L. T. (2012). Network-specific effects of age and in-scanner subject motion: a resting-state fMRI study of 238 healthy adults. *NeuroImage, 63(3),* 1364–73.

Nachman, S., Chernoff, M., Williams, P., Hodge, J., Heston, J., & Gadow, K. D. (2012). Human Immunodeficiency Virus Disease Severity, Psychiatric Symptoms, and Functional Outcomes in Perinatally Infected Youth. *Archives of Pediatrics & Adolescent Medicine, 166(6),* 528.

Neter, J., Wasserman, W. & Kutner, M. H. (1989). *Applied Linear Regression Models.* Homewood, IL: Irwin.

Nozyce, M.L., Lee, S.S., Wiznia, A., Nachman, S., Mofenson, L.M., Smith, M.E., Yogev, R., McIntosh, K., Stanley, K., & Pelton, S. (2006). A behavioral and cognitive profile of clinically stable HIV-infected children. *Pediatrics, 117(3),* 763–70.

Ossandon, T., Vidal, J.R., Ciumas, C., Jerbi, K., Hamame, C.M., Dalal, S.S., Bertrand, O., Minotti, L., Kahane, P., & Lachaux, J.-P. (2012). Efficient “Pop-Out” Visual Search Elicits Sustained Broadband Gamma Activity in the Dorsal Attention Network. *Journal of Neuroscience, 32(10),* 3414–3421.

Ozaki, T. J. (2011). Frontal-to-parietal top-down causal streams along the dorsal attention network exclusively mediate voluntary orienting of attention. *PLoS ONE, 6(5),* 1–9.

Palchetti, C. Z., Patin, R. V., Gouvêa, A. de F. T. B., Szejnfeld, V. L., Succi, R. C. D. M., & Oliveira, F. L. C. (2012). Body composition and lipodystrophy in prepubertal HIV-infected children. *The Brazilian Journal of Infectious Diseases, 17(1),* 1–6.

Pasquale, F. de, Penna, S. Della, Snyder, A. Z., Marzetti, L., Pizzella, V., Romani, G. L., & Corbetta, M. (2012). A cortical core for dynamic integration of functional networks in the resting human brain. *Neuron, 74(4),* 753–764.

Patel, K., Ming, X., Williams, P. L., Robertson, K. R., Oleske, J. M., & Seage, G.R. (2009). Impact of HAART and CNS-penetrating antiretroviral regimens on HIV encephalopathy among perinatally infected children and adolescents. *Journal of Acquired Immune Deficiency Syndromes, 23(14),* 1893–1901.

Pavlakis, S.G., Lu, D., Frank, Y., Bakshi, S., Pahwa, S., Barnett, T. a, Porricolo, M.E., Gould, R.J., Nozyce, M.L., & Hyman, R. A., (1995). Magnetic resonance spectroscopy in childhood AIDS encephalopathy. *Pediatric Neurology, 12(95),* 277–282.

Piccoli, T., Valente, G., Linden, D. E. J., Re, M., Esposito, F., Sack, A. T., & Salle, F. Di. (2015). The Default Mode Network and the Working Memory Network Are Not Anti-Correlated during All Phases of a Working Memory Task. *Plos One, 10(4),* 1–16.

Prado, P. T. C., Escorsi-Rosset, S., Cervi, M. C., & Santos, A. C. (2011). Image evaluation of HIV encephalopathy: a multimodal approach using quantitative MR techniques. *Neuroradiology, 53(11),* 899–908.

Prince, Jerry. (2006). *Medical Imaging and systems*. Upper Saddle River, N.J.: Pearson Prentice Hall.

Ptak, R. (2012). The Frontoparietal Attention Network of the Human Brain: Action, Saliency, and a Priority Map of the Environment. *The Neuroscientist, 18(5),* 502–515.

Purohit, V., Rapaka, R. S., Schnur, P., & Shurtleff, D. (2011). Potential impact of drugs of abuse on mother-to-child transmission (MTCT) of HIV in the era of highly active antiretroviral therapy (HAART). Life Sciences, 88, 909–16.

Pyka, M., Beckmann, C.F., Schöning, S., Hauke, S., Heider, D., Kugel, H., Arolt, V., & Konrad, C. (2009). Impact of working memory load on fMRI resting state pattern in subsequent resting phases. *PLoS ONE, 4(9),* 1–7.

Qiu, W., Yan, B., Tong, L., Wang, L., & Shi, D. (2011).A resting-state fMRI study of patients with HIV infection based on regional homogeneity method. *Seventh International Conference on Natural Computation,* 997–1000.

Raichle, M. E., MacLeod, A. M., Snyder, A. Z., Powers, W. J., Gusnard, D. A, & Shulman, G. L. (2001). A default mode of brain function. *Proceedings of the National Academy of Sciences, 98(2),* 676–82.

Raskino, C., Pearson, D. A., Baker, C. J., Lifschitz, M. H., Donnell, O., Mintz, M., Nozyce, M., Brouwers, P., Mckinney, R. E., & Jimenez, E. (1999). Neurologic, Neurocognitive, and Brain Growth Outcomes in Human Immunodeficiency Virus-Infected Children receiving different nucleoside antiretroviral regimens. *Pediatrics, 104(3),* 1–10.

Rogers, B. P., Morgan, V. L., Newton, A. T., & Gore, J. C. (2007).Assessing functional connectivity in the human brain by fMRI. *Magnetic Resonance Imaging, 25(10),* 1347–1357.

Ruel, T.D., Boivin, M.J., Boal, H.E., Bangirana, P., Charlebois, E., Havlir, D. V., Rosenthal, P.J., Dorsey, G., Achan, J., Akello, C., Kamya, M.R., & Wong, J.K. (2012). Neurocognitive and motor deficits in HIV-infected ugandan children with high CD4 cell counts. *Clinical Infectious Diseases, 54,* 1001–1009.

Saitoh, A., Singh, K.K., Sandall, S., Powell, C. a, Fenton, T., Fletcher, C. V, Hsia, K., & Spector, S. A. (2006). Association of CD4+ T-lymphocyte counts and new thymic emigrants in HIV-infected children during successful highly active antiretroviral therapy. *The Journal of Allergy and Clinical Immunology, 117(4),* 909–15.

Sarma, M.K., Nagarajan, R., Keller, M. A., Kumar, R., Nielsen-Saines, K., Michalik, D.E., Deville, J., Church, J. A, & Thomas, M.A. (2013). Regional brain gray and white matter changes in perinatally HIV-infected adolescents. *NeuroImage. Clinical, 4,* 29–34.

Seeley, W.W., Menon, V., Schatzberg, A.F., Keller, J., Glover, G.H., Kenna, H., Reiss, A.L., & Greicius, M.D. (2007). Dissociable intrinsic connectivity networks for salience processing

and executive control. *The Journal of Neuroscience, 27(9),* 2349–56. doi:10.1523/JNEUROSCI.5587-06.2007

Sestieri, C., Corbetta, M., Romani, G. L., & Shulman, G. L. (2011). Episodic memory retrieval, parietal cortex, and the Default Mode Network: functional and topographic analyses. *Journal of Neuroscience, 31(12),* 4407–4420.

Shanbhag, M. C., Rutstein, R. M., Zaoutis, T., Zhao, H., Chao, D., & Radcliffe, J. (2005). Neurocognitive Functioning in Pediatric Human Immunodeficiency Virus Infection - effects of combined therapy. *Archives of Pediatrics & Adolescent Medicine, 159,* 651–656.

Sheon, A.R., Fox, H.E., Rich, K.C., Stratton, P., Diaz, C., Tuomala, R., Mendez, H., Carrington, J., & Alexander, G. (1996). The Women and Infants Transmission Study (WITS) of Maternal-Infant HIV Transmission: Study Design, Methods, and Baseline Data. *Journal of Women's Health, 5(1),* 69–78.

Sherr, L., Mueller, J., & Varrall, R. (2009). A systematic review of cognitive development and child human immunodeficiency virus infection. *Psychology, Health & Medicine*, *14*(4), 387–404.

Smith, A. M., Lewis, B. K., Ruttimann, U. E., Ye, F. Q., Sinnwell, T. M., Yang, Y., Duyn, J. H., & Frank, J. A. (1999). Investigation of low frequency drift in fMRI signal. *Neuroimage, 9,* 526–533.

Smith, S.M., Jenkinson, M., Woolrich, M.W., Beckmann, C.F., Behrens, T.E.J., Johansen-Berg, H., Bannister, P.R., De Luca, M., Drobnjak, I., Flitney, D.E., Niazy, R., Saunders, J., Vickers, J., Zhang, Y., De Stefano, N., Brady, J.M., & Matthews, P.M. (2004). Advances in functional and structural MR image analysis and implementation as FSL. *NeuroImage, 23,* S208-19.

Smith, R., Malee, K., Leighty, R., Brouwers, P., Mellins, C., Hittelman, J., Chase, C., & Blasini, I. (2006). Effects of perinatal HIV infection and associated risk factors on cognitive development among young children. *Pediatrics, 117(3*), 851–62.

Smith, S., Fox, P., Miller, K.L., Glahn, D.C., Fox, P.M., Mackay, C.E., Filippini, N., Watkins, K.E., Toro, R., Laird, A.R., & Beckmann, C.F. (2009). Correspondence of the brain's functional

architecture during activation and rest. *Proceedings of the National Academy of Science, 106(31),* 13040–13045.

Smith, R., Chernoff, M., Williams, P.L., Malee, K.M., Sirois, P.A., Kammerer, B., Wilkins, M., Nichols, S., Mellins, C., Usitalo, A., Garvie, P., & Rutstein, R. (2012). Impact of Human Immunodeficiency Virus Severity on Cognitive and Adaptive Functioning during Childhood and Adolescence. *Pediatric Infectious Diseases, 31(6),* 1–11.

Soberman, R., Brodie, B. B., Levy, B. B., Axelrod, J., Hollander, V., & Steele, J. M. (1948). The use of antipyrine in the measurement of total body water in man. *The Journal of Biological Chemistry, 179,* 31–42.

Statistics South Africa, 2013. *Mid-year population estimates,* Available from: http://www.statssa.gov.za/publications/P0302/P03022013.pdf.

Stout, J.C., Ellis, R.J., Jernigan, T.L., Archibald, S.L., Abramson, I., Wolfson, T., McCutchan, A., Wallace, M.R., Atkinson, & J.H., Grant, I. (1998). Progressive Cerebral Volume Loss in Human Immunodeficiency Virus Infection. *American Medical Association, 55,* 161–168.

Superkar, K., Musen, M., & Menon, V. (2009). Development of Large-Scale Functional Brain Networks in Children. *PLoS Biology, 7(7),* 1–15.

Superkar, K., Uddin, L. Q., Prater, K., Amin, H., Greicius, M. D., & Menon, V. (2010). Development of functional and structural connectivity within the default mode network in children. *Neuroimage, 52,* 290–301.

Tahan, T. T., Bruck, I., Burger, M., & Cruz, C. R. (2006). Neurological profile and neurodevelopment of 88 children infected with HIV and 84 seroreverter children followed from 1995 to 2002. *The Brazilian Journal of Infectious Diseases, 10,* 322–326.

Tangsinmankong, N., Kamchaisatian, W., Lujan-Zilbermann, J., Brown, C.L., Sleasman, J.W., & Emmanuel, P.J. (2004). Varicella zoster as a manifestation of immune restoration disease in HIV-infected children. *The Journal of Allergy and Clinical Immunology, 113(4),* 742–6.

Tardieu, M., Mayaux, M.-J., Seibel, N., Funck-Brentano, I., Straub, E., Teglas, J.-P., & Blanche, S. (1995). Cognitive assessment of school-age children infected with maternally

transmitted human immunodeficiency virus type. *The Journal of Pediatrics, 126(3),* 375–379.

Taylor, P., & Saad, Z. (2013). FATCAT: (An Efficient) Functional And Tractographic Connectivity Analysis Toolbox. *Brain Connectivity, 3(5),* 523–535.

Taylor, J. M., Fahey, J. L., Detels, R., & Giorgi, J. V. (1989). CD4 Percentage, CD4 Number, and CD4:CD8 ratio in HIV infection: which to choose and how to use. *Journal of Acquired Immune Deficiency Syndromes, 2,* 114–124.

South African antiretroviral treatment Guildelines (2013). Available from: http://www.sahivsoc.org/upload/documents/2013%20ART%20Guidelines-Short%20Combined%20FINAL%20draft%20guidelines%2014%20March%202013.pdf

Taipale, A., Pelkonen, T., Taipale, M., Roine, I., Bernardino, L., Peltola, H., & Pitkäranta, A. (2011). Otorhinolaryngological findings and hearing in HIV-positive and HIV-negative children in a developing country. *European Archives of Oto-Rhino-Laryngology, 268(10),* 1527–1532.

Thomaidis, L., Bertou, G., Critselis, E., Spoulou, V., Kafetzis, D. A., & Theodoridou, M. (2010). Cognitive and psychosocial development of HIV pediatric patients receiving highly active anti-retroviral therapy: a case-control study. *BMC Pediatrics, 10*, 1–9.

Thomas, J. B., Brier, M. R., Snyder, A. Z., Vaida, F. F., & Ances, B. M. (2013). Pathways to neurodegeneration: effects of HIV and aging on resting-state functional connectivity. *Neurology, 80(13),* 1186–93.

Thomason, M.E., Dennis, E.L., Joshi, A. a, Joshi, S.H., Dinov, I.D., Chang, C., Henry, M.L., Johnson, R.F., Thompson, P.M., Toga, A.W., Glover, G.H., Van Horn, J.D., & Gotlib, I.H. (2011). Resting-state fMRI can reliably map neural networks in children. *NeuroImage, 55(1),* 165–75.

Thompson, P. M., Dutton, R. A., Hayashi, K. M., Toga, A. W., Lopez, O. L., Aizenstein, H. J., & Becker, J. T. (2005). Thinning of the cerebral cortex visualized in HIV¯AIDS reflects CD4+ T lymphocyte decline. *Proceedings of the National Academy of Science, 102(43),* 15647–15652.

Tisdall, M.D., Hess, A. T., & van der Kouwe, A. J. W. (2009). MPRAGE Using EPI Navigators for Prospective Motion Correction. ISMRM.:Honolulu, HI. p. 4656.

UNAIDS. (2012). Sub-Saharan Africa - AIDS epidemic facts and figures. Available from: http://www.unaids.org/en/media/unaids/contentassets/documents/epidemiology/2012/gr2012/2012_FS_regional_ssa_en.pdf

UNAIDS. (2013). Global AIDS epidemic fact and figures, Available from: http://www.unaids.org/en/resources/presscentre/factsheets/.

Van der Kouwe, A.J. W., Benner, T., Salat, D.H., & Fischl, B. (2008). Brain morphometry with multiecho MPRAGE. *Neuroimage, 40*, 559-569.

Van Rie, A., Harrington, P. R., Dow, A., & Robertson, K. (2006). Neurologic and neurodevelopmental manifestations of pediatric HIV/AIDS: a global perspective. European *Journal of Paediatric Neurology, 11(1),* 1–9.

Van Rie, A., Mupuala, A., & Dow, A. (2008). Impact of the HIV/AIDS epidemic on the neurodevelopment of preschool-aged children in Kinshasa, Democratic Republic of the Congo. *Pediatrics, 122(1),* e123–8.

Van Rie, A., Dow, A, Mupuala, A., & Stewart, P. (2009). Neurodevelopmental trajectory of HIV-infected children accessing care in Kinshasa, Democratic Repulic of Congo. *Journal of Acquired Immune Deficiency Syndromes, 52(5),* 636–642.

Violari, A., Cotton, M. F., Gibb, D. M., Babiker, A. G., Steyn, J., Madhi, S. A., Jean-Philippe, P., & McIntyre, J. a. (2008). Early antiretroviral therapy and mortality among HIV-infected infants. *The New England Journal of Medicine, 359(21),* 2233–44.

Vogel, A. C., Miezin, F. M., Petersen, S. E., & Schlaggar, B. L. (2012). The putative visual word form area is functionally connected to the dorsal attention network. *Cerebral Cortex, 22,* 537–549.

Wachsler-Felder, J. L., & Golden, C. J. (2002). Neuropsychological consequences of HIV in children: a review of current literature. *Clinical Psychology Review, 22(3),* 443–64.

Wang, K., Liang, M., Wang, L., Tian, L., Zhang, X., Li, K., & Jiang, T. (2007).Altered functional connectivity in early Alzheimer's disease: a resting-state fMRI study. *Human Brain Mapping, 28(10),* 967–78.

Wang, L., Zang, Y., He, Y., Liang, M., Zhang, X., Tian, L., Wu, T., Jiang, T., & Li, K. (2006). Changes in hippocampal connectivity in the early stages of Alzheimer's disease: evidence from resting state fMRI. *NeuroImage, 31(2),* 496–504.

Weissman, D. H., & Prado, J. (2012). Heightened activity in a key region of the ventral attention network is linked to reduced activity in a key region of the dorsal attention network during unexpected shifts of covert visual spatial attention. *NeuroImage, 61(4),* 798–804.

Westmoreland, S. V, Rottman, J. B., Williams, K. C., Lackner, A. A., & Sasseville, V. G. (1998). Chemokine Receptor Expression on Resident and Inflammatory Cells in the Brain of Macaques with Simian Immunodeficiency Virus Encephalitis. *American Journal of Pathology, 152(3),* 659–665.

Wolters, P. L., Brouwers, P., Moss, H. A., & Pizzo, P. A. (1995). Differential receptive and expressive language functioning of children with symptomatic HIV disease and relation to CT scan brain abnormalities. *Pediatrics, 95(1),* 112–119.

Woolrich, M.W., Jbabdi, S., Patenaude, B., Chappell, M., Makni, S., Behrens, T., Bechmann, C., Jenkinson, M., & Smith, S.M. (2009). Bayesian analysis of neuroimaging data in FSL. *NeuroImage, 45,* S173-86

World Health Organization. (2013a). Treatment of children living with HIV. Available from: http://www.who.int/hiv/topics/paediatric/en/

World Health Organization. (2013b). Mother-to-child transmission of HIV. Available from: http://www.wpro.who.int/hiv/topics/pmtct/about/en/

Xiong, J., Parsons, L. M., Gao, J. H., & Fox, P. T. (1999). Interregional connectivity to primary motor cortex revealed using MRI resting state images. *Human Brain Mapping, 8,* 151–6.

Yan, C.-G., Cheung, B., Kelly, C., Colcombe, S., Craddock, R.C., Di Martino, A., Li, Q., Zuo, X.-N., Castellanos, F.X., & Milham, M.P. (2013). A comprehensive assessment of regional variation in the impact of head micromovements on functional connectomics. *NeuroImage, 76,* 183–201.

Ye, P., Kirschner, D. E., & Kourtis, A. P. (2004). The thymus during HIV disease: role in pathogensis and in immune recovery. *Current HIV Research, 2,* 177–183.

Yeo, B.T.T., Krienen, F.M., Sepulcre, J., Sabuncu, M.R., Lashkari, D., Hollinshead, M., Roffman, J.L., Smoller, J.W., Zollei, L., Polimeni, J.R., Fischl, B., Liu, H., & Buckner, R.L. (2011). The organization of the human cerebral cortex estimated by intrinsic functional connectivity. *Journal of Neurophysiology, 106,* 1125–1165.

Zatorre, R. J., Belin, P., & Penhune, V. B. (2002). Structure and function of auditory cortex: music and speech. *Trends in Cognitive Sciences, 6(1),* 37–46.

Zou, Q., Wu, C. W., Stein, E. a., Zang, Y., & Yang, Y. (2009). Static and dynamic characteristics of cerebral blood flow during the resting state. *NeuroImage, 48(3),* 515–524.